Practical model for predicting corrosion rate of steel reinforcement in concrete structures

Yu, Bo; Yang, LuFeng; Wu, Ming; Li, Bing

2013

Yu, B., Yang, L., Wu, M., & Li, B. (2014). Practical model for predicting corrosion rate of steel reinforcement in concrete structures. Construction and Building Materials, 54, 385-401.

https://hdl.handle.net/10356/103466

https://doi.org/10.1016/j.conbuildmat.2013.12.046

Practical Model for Predicting Corrosion Rate of Steel Reinforcement in Concrete Structures

Bo YU [1], **LuFeng YANG** [2], **Ming WU** [3] and **Bing LI** [4]

Abstract: A practical model for predicting corrosion rate of steel reinforcement in concrete structures was proposed. The numerical model with nonlinear boundary conditions for macrocell corrosion of steel reinforcement in concrete structures was established based on electrochemical principles and the Bulter-Volmer equation. The influences of parameters such as anode-to-cathode (A/C) ratio, relative humidity, concrete resistivity, cover thickness on the corrosion control mode and corrosion rate of steel reinforcement in concrete structures were then investigated. Finally, a practical model for predicting corrosion rate of steel reinforcement in concrete structures was proposed based on a comprehensive nonlinear regression analysis with easily quantifiable engineering parameters, such as water-to-cement (W/C) ratio, chloride content, thickness of concrete cover and relative humidity. Model comparison and experimental verification demonstrate that the proposed prediction model is of good accuracy and applicability to real life scenarios in terms of capturing the corrosion behavior of steel reinforcement in different situations.

Keywords: reinforced concrete; corrosion rate; concrete resistivity; cover thickness; water-to-cement ratio; chloride content; relative humidity

Highlights:

- The influences of anode-to-cathode ratio, relative humidity, concrete resistivity, and cover thickness on control mode and corrosion rate of steel reinforcement were investigated.
- Potential difference between concrete surface and steel/concrete interface for both uniform and pitting corrosions was presented.
- Advantages and disadvantages of increment of cover thickness on both corrosion initiation and propagation in different situations were discussed.
- A practical prediction model of corrosion rate for steel reinforcement in concrete structures with easily quantifiable engineering parameters was proposed.

- Model comparison and experimental validation of prediction models for corrosion rate of steel reinforcement in concrete structures were performed.

---

[1] Associate Professor, Key Laboratory of Disaster Prevention and Structural Safety of Ministry of Education of the P. R. China, School of Civil Engineering & Architecture, Guangxi University, Nanning, China, 530004

[2] Professor, Agency of Housing and Urban-Rural Development, Guangxi Autonomous Zhuang Region, Nanning, China, 530028; Key Laboratory of Disaster Prevention and Structural Safety of Ministry of Education of the P. R. China, Guangxi University, Nanning, China, 530004 (Corresponding author: lfyang@gxu.edu.cn)

[3] Master of Structural Engineeing, School of Civil Engineering & Architecture, Guangxi University, Nanning, China, 530004

[4] Director and Associate Professor, Natural Hazard Research Centre (NHRC), Nanyang Technological University, Singapore, 639798

1. Introduction

Deterioration of reinforced concrete (RC) structures due to carbonation or chloride ingress induced corrosion of steel reinforcement is a major concern for infrastructure owners and operators [1]. The service life of RC structures with respect to corrosion of steel reinforcement is usually divided into two distinct phases – the corrosion initiation and the corrosion propagation [2]. The former refers to the depassivation of steel reinforcement induced by the ingress and accumulation of aggressive agents such as chloride ions and carbon dioxide, while the latter starts from corrosion of steel reinforcement to structural failure induced by cracking/spalling of concrete cover or steel bar strength degradation. Corrosion rate of steel reinforcement not only determines the speed of formation and accumulation for corrosion products which influences the performance of concrete cover and serviceability of RC structures, but also controls the reduction rate of effective cross-section area of steel bar and load-bearing capacity of RC structures. Hence, corrosion rate of steel reinforcement plays an important role in safety evaluation, maintenance decision and residual life prediction of existing RC structures.

Over the past several decades, corrosion of steel reinforcement in concrete structures has been widely investigated and various prediction models including empirical models, reaction control models (oxygen diffusion or concrete resistivity) and electrochemical models for corrosion rate of steel reinforcement have been proposed [3].

Empirical models are mainly based on the assumed direct relationships between corrosion rate and basic structural parameters (e.g. water-to-cement (W/C) ratio, binder type, thickness of concrete cover, *et al*.) and environmental parameters (e.g. temperature, relative humidity, chloride concentration, *et al*.). The unknown coefficients of empirical models are usually determined by referring to the relevant experimental data. Liu and Weyers [4] proposed a nonlinear regression model for corrosion rate as a function of chloride content, temperature, ohmic resistance of concrete cover, and active corrosion time, based on the measured corrosion parameters of forty four bridge deck slabs over a five-year outdoor exposing period. It is clear that this model ignores the influence of oxygen and adopts ohmic resistance of concrete cover as a governing parameter which causes the prediction model to be

geometry dependent. Scott *et al.* [5] discussed the influences of binder type, thickness of concrete cover and crack width on corrosion rate of steel reinforcement in the cracked concrete prismatic specimens, based on seven concrete mixtures comprising ordinary Portland cement (OPC) and blends of the OPC with different supplementary cementitious materials. Jiang *et al.* [6] carried out an accelerated corrosion experiment on reinforced concrete specimens in a computer-controlled chamber and fitted a prediction model of the corrosion rate by taking temperature, relative humidity, thickness of concrete cover, W/C ratio into account. Yu *et al.* [7] investigated the influences of W/C ratio, thickness of concrete cover, chloride content, mineral admixtures on corrosion rate, but the influence of relative humidity was ignored. Zhu *et al.* [8] proposed an empirical model to describe the relationship between corrosion rate and concrete resistance as well as corrosion potential, based on the corrosion parameters detected by the linear polarization device Gecor 6. However, it fails to consider the influence of oxygen and is geometry dependent. Although empirical model is simple and convenient for engineers, it is often limited to the set of conditions under which they are developed. Since selected variables under consideration are investigated in isolation from other influencing parameters and/or the interaction thereof [2].

Reaction control models assume that electrical resistivity (ion transportation) and oxygen diffusion resistance (cathodic reaction) of concrete cover are two major controlling factors for the corrosion of steel reinforcement in concrete structures. They indirectly take into account other influencing factors such as temperature, relative humidity, W/C ratio and binder type, *et al*. Vu *et al.* [9] assumed that corrosion of steel reinforcement in concrete structures was limited by the availability of oxygen at the steel surface and established a prediction model of corrosion rate as a function of W/C ratio and cover thickness when relative humidity is 75% and temperature is 20℃. Although the influence of oxygen supply is reflected in the prediction model, it neglects concrete electrical resistivity and therefore is only suitable for corrosion of steel reinforcement under control of cathodic reaction. Based on the assumption that the concrete was water saturated and corrosion of steel reinforcement was under control of oxygen diffusion, Huet *et al.* [10] established a prediction model for corrosion rate as a function of porosity, oxygen concentration, degree of water saturation, and oxygen diffusion coefficient in concrete pore liquid. Furthermore, Alonso *et al.* [11] established an empirical

relationship between corrosion rate and concrete electrical resistivity by fitting the experimental data. Although reaction control models consider the influence of oxygen diffusion (cathodic reaction) or concrete resistivity (ion transportation) on corrosion rate, the unknown coefficients of prediction models are mainly determined by fitting the experimental data and these models belong to quasi-empirical models in nature.

Electrochemical models are based on electrochemical principles of corrosion and establish prediction model of corrosion rate with electrochemical parameters. Stern *et al.* [12] found a linear dependence of potential on logarithmic scales of applied current for small amounts of polarization in experiment. Consequently they proposed the linear polarization theory which determines the corrosion rate when the anodic/cathodic Tafel slope and the polarization resistance were known. Using the equivalent circuit approach set up for a well-defined two-dimensional geometry, Raupach *et al.* [13] calculated corrosion rate with the anodic/cathodic polarization resistance, concrete resistance, and the anodic/cathodic equilibrium potential. Isgor *et al.* [14] built a macrocell corrosion model for steel reinforcement in concrete structures by considering both the anodic/cathodic activation polarization and the cathodic diffusion polarization. Li *et al.* [15] established a modified macrocell corrosion model by considering the inpact of rebar stress on corrosion rate. Cao *et al.* [16] built a prediction model which could consider both the macrocell and microcell corrosion simultaneously, based on the examination of the anodic/cathodic activation polarization and the cathodic diffusion polarization. Yu *et al.* [17] investigated the influences of cover thickness, concrete resistivity and degree of pore saturation of concrete on the corrosion mechanism and the corrosion rate of steel reinforcement in concrete structures based on the macrocell corrosion model. Generally, electrochemical models are rigorously established and could comprehensively reflect corrosion mechanism if the electrochemical parameters are selected rightly. However, electrochemical models are computationally time-consuming and too complex to be adopted by the general engineering community.

Although a large number of prediction models for corrosion rate of steel reinforcement in concrete structures have already been developed, lots of challenges remain such as the determination of electrochemical parameters, numerical difficulties in solution of governing equations due to nonlinear boundary conditions and complicacies in modelling complicated

geometries (e.g. reinforcement details) and non-homogeneous material properties, *et al*. Therefore, a practical model of sufficient accuracy and easy application in terms of predicting corrosion rate of steel reinforcement in concrete structures is desirable. The main objective of this study is to develop a practical model for predicting corrosion rate of steel reinforcement in concrete structures with easily quantifiable engineering parameters. The influences of important engineering parameters, such as anode-to-cathode (A/C) ratio, relative humidity, concrete resistivity, thickness of concrete cover, *et al*., on the corrosion control mode and the corrosion rate of steel reinforcement were investigated first based on the numerical model of macrocell corrosion. Then a practical model for predicting corrosion rate of steel reinforcement in concrete structures was proposed based on a comprehensive nonlinear regression analysis with easily quantifiable engineering parameters, such as W/C ratio, chloride content, thickness of concrete cover and relative humidity. Finally, both model comparison and experimental validation to demonstrate the accuracy and practicality of the proposed prediction model were performed.

2. Macrocell corrosion model of steel reinforcement in concrete

2.1. Corrosion mechanism of steel reinforcement in concrete

Corrosion of steel reinforcement in concrete structures is a complicated electrochemical process. As newly cast concrete is highly alkaline, a passive film can form on the steel surface, which will prevent initiation of corrosion of steel reinforcement. However, the passive film gradually dissolves with the ingress and accumulation of carbon dioxide or chloride ions within concrete cover, which will generate potential difference between active and passive regions at the steel surface. If water and oxygen are adequate near the steel/concrete interface, corrosion of steel reinforcement will start, as shown in Fig. 1.

In the activated region, the iron atom leaves the lattice and turns into atom absorbed onto the steel surface, which will go through the electrical double layer, discharge and be oxidized. Therefore anode forms in this region, and the corresponding reaction equation is

$$\mathrm{Fe} \rightarrow \mathrm{Fe}^{2+} + 2\mathrm{e}^{-} \tag{1}$$

At the interface between passive steel and concrete, electrons from anode are consumed

by oxygen and water to preserve electrical neutrality, which are reduced into OH^-. Here cathode of macrocell corrosion forms, and the corresponding reaction equation is

$$O_2 + 4e^- + 2H_2O \rightarrow 4OH^- \tag{2}$$

Reactants consisting of Fe^{2+} and OH^- generated by anodic and cathodic reactions further react with each other, which forms $Fe(OH)_2$ as follows

$$Fe^{2+} + 2OH^- \rightarrow Fe(OH)_2 \tag{3}$$

Provided that oxygen supply is enough, $Fe(OH)_2$ can transform into $Fe(OH)_3$, which will become loose porous Fe_2O_3 after dehydration, as shown in below

$$4Fe(OH)_2 + O_2 + 2H_2O \rightarrow 4Fe(OH)_3 \tag{4}$$

$$2Fe(OH)_3 \rightarrow Fe_2O_3 + 3H_2O \tag{5}$$

When oxygen supply is insufficient, $Fe(OH)_2$ will transform into Fe_3O_4 by

$$6Fe(OH)_2 + O_2 \rightarrow 2Fe_3O_4 + 6H_2O \tag{6}$$

Corrosion of steel reinforcement in concrete structures causes the decrease of the effective cross-section area of reinforcing steel. Besides, the expansion of reactants leads to the cracking/spalling of concrete cover and bond-slip between concrete and steel. Finally both serviceability and ultimate bearing capacity of RC structure will degenerate.

2.2. Modeling corrosion of steel reinforcement in concrete

As shown in Fig. 2, the concrete cover on the lower part of RC beam cracks under the action of the perpendicular load which forms a convenient passage for the entry of corrosive substances, such as chloride ions and carbon dioxide. Therefore, the concentration of aggressive agents around steel surface increases gradually. Finally the destruction of passive film and corrosion of steel reinforcement appear. As the RC structure is symmetrical, a typical zone with cover thickness of d and length of L at the right side of RC beam is considered in this study for simplicity. Furthermore, the lengths of anode and cathode for macrocell corrosion model are assumed to be L_a and L_c respectively.

When steel reinforcement corrodes, the transfer of electrons and ions will induce a net current to flow through the electrodes and anodic/cathodic corrosion potential will deviate

from its equilibrium potential. This change in potential is called as the polarization, including the activation polarization, the concentration polarization and the resistance polarization [18].

At the anodic site, the reaction products diffuse so fast that the concentration polarization is usually negligible. Meanwhile, resistance of steel is much less than that of concrete and the resistance polarization can be ignored since the passive film at the anodic site has already been broken. So the anodic reaction is dependent on an increment in the potential to overcome the activation energy of the reaction. For the corrosion of steel reinforcement in concrete, the anodic corrosion potential E_a can be expressed as

$$E_a = E_a^0 + \beta_a \log \frac{i_a}{i_{0a}} \tag{7}$$

where, E_a^0 is the anodic equilibrium potential (V); i_a is the anodic current density (A/m^2); i_{0a} is the anodic exchange current density (A/m^2); β_a is the anodic Tafel slope (V).

As cathodic reaction occurs outside the passive film, the resistance polarization is negligible. So the cathodic reaction is controlled by two kinds of polarizations – the activation polarization induced by the slow entrance of electron into the electrode and the concentration polarization caused by the limited supply of oxygen or diffusion of reaction products. Generally, the cathodic reaction is controlled by a combined polarization — that is, activation polarization at lower reaction rate and concentration polarization at higher reaction rate. Hence, the cathodic corrosion potential E_c can be described as

$$E_c = E_c^0 + \beta_c \log \frac{i_c}{i_{0c}} - \frac{2.303RT}{nF} \log \frac{i_L}{i_L - i_c} \tag{8}$$

where, E_c^0 is the cathodic equilibrium potential (V); i_{0c} is the cathodic current density (A/m^2); i_{0c} is the cathodic exchange current density (A/m^2); β_c is the cathodic Tafel slope (V); i_L is the limit current density (A/m^2); F is the Faraday's constant, F=96494C; R is the universal gas constant, R=8.314 J/(K mol); T is the absolute temperature (K).

Assuming that the concrete matrix is isotropic and homogeneous with respect to electrical resistivity and diffusion coefficient of oxygen, and corrosion of steel reinforcement is not influenced by the external electric field, the distribution of corrosion potential within

two-dimensional concrete cover can be described as [14, 17]

$$\frac{\partial^2 E}{\partial x^2}+\frac{\partial^2 E}{\partial y^2}=0 \tag{9}$$

where, E is the corrosion potential; x and y are coordinates.

According to the Ohm's law, the current density at any point within concrete cover is

$$i=-\frac{1}{\rho}\frac{\partial E}{\partial n} \tag{10}$$

where, i is the corrosion current density (A/m^2); n is the direction normal to the equipotential lines; ρ is the electrical resistivity of concrete cover (Ω•m).

During the corrosion process of steel reinforcement, the cathodic concentration polarization is mainly controlled by the oxygen diffusion. Assuming that diffusion of oxygen within concrete follows the Fick's first law and oxygen doesn't retain at the steel surface, the limit current density i_L can be defined by

$$i_L=n_e F\frac{D_{O_2}C_{s,O_2}}{\delta} \tag{11}$$

where, n_e is the number of electrons exchanged in the cathodic reaction, n_e=4; D_{O_2} is effective oxygen diffusion coefficient in concrete cover (m^2/s); C_{s,O_2} is the oxygen concentration in concrete pore solution near the steel surface and around the cathodic region; δ is the effective thickness of oxygen diffusion layer (m).

As shown in Fig. 2, the distribution of corrosion potential within concrete cover can be determined by solving the Eq. (9) with the boundary conditions defined by the Eqs. (7) and (8). Since both anodic and cathodic current densities in the Eqs. (7) and (8) are unknown in advance, the Eq. (9) cannot be solved explicitly. The iterative solution strategy developed in this study is as follows:

1. Select initial values for anodic and cathodic current densities (i_a and i_c) and substitute them into the Eqs. (7) and (8) to determine both anodic and cathodic boundary conditions (E_a and E_c);
2. Calculate the distribution of corrosion potential (E) within concrete cover by solving the Eq. (9) with both anodic and cathodic boundary conditions determined by the step 1;

3. Calculate the current density (i) at every discrete node on the steel surface according to the Eq. (10). Here, anodic and cathodic current densities are denoted as i_a and i_c, respectively;
4. Judge the magnitude between i_c and i_L. If $i_c > i_L$, i_c should be modified to satisfy $i_c \le i_L$, and i_a should be adjusted according to the conservation of charge. If $i_c \le i_L$, goes to the step 5;
5. Substitute the calculated anodic and cathodic current densities (i_a and i_c) into the Eqs. (7) and (8) to update both anodic and cathodic boundary conditions (E_a and E_c);
6. Recalculate the distribution of corrosion potential (E) within concrete cover by solving the Eq. (9) with the updated anodic and cathodic boundary conditions;
7. Recalculate the corrosion current densities (i_a and i_c) by solving the Eq. (10) using the new corrosion potential;
8. Repeat the steps 4～7 until the relative errors of corrosion potential (E) and corrosion current density (i) calculated in the adjacent two iterative steps are lower than the predefined allowable values.

The detailed procedure for the solution of nonlinear numerical model for macrocell corrosion is illustrated in Fig. 3. Based on the numerical model described above, the distribution of potential within concrete cover and the corrosion rate on the steel surface can be determined. Furthermore, the effect of influential parameters such as the electrical resistivity of concrete, thickness of concrete cover, and relative humidity on the potential distribution and the corrosion rate can be investigated quantificationally.

Corrosion rate of steel reinforcement is usually expressed by the mean of corrosion current density at the anodic region, which can be expressed as

$$i_m = \frac{I_{corr}}{L_a} = \frac{1}{L_a}\int_0^{L_a} i_a dx \tag{12}$$

where, i_m is the mean of corrosion current density at the anodic region; I_{corr} is the corrosion current intensity.

The macrocell corrosion model described by the Eqs. (7) to (12) contains 8

electrochemical parameters. According to electrochemical principles of corrosion [19], the anodic Tafel slope (β_a) is usually between 30mV and 120mV for corrosion of steel reinforcement, while the cathodic Tafel slope (β_c) is about −120mV for iron or plain low carbon steel corroded in acid solution. The magnitude of the exchange current density is within 10^{-4}A/m^2 to 10^{-5}A/m^2 when the concentration of Fe^{2+} is 1mol/L. Concrete resistivity (ρ) can vary in a wide range as much as several orders of magnitude for different environmental conditions. According to work by Polder *et al.* [20], electrical resistivity of the ordinary Portland cement concrete is usually between 50Ω•m and 200Ω•m for RC structures directly contact with water, between 100Ω•m and 400Ω•m for those exposed in air without any surface protection, between 200Ω•m to 500Ω•m for those exposed in air with surface protection, and no less than 3000Ω•m for those in arid indoor environment. However, the probability of corrosion of steel reinforcement is negligible when the concrete electrical resistivity is relatively large (e.g. ρ >1000Ω•m). In the present study, the concrete resistivity is considered to vary between 5 and 1400Ω•m (9 values: 5, 50, 200, 400, 600, 800, 1000, 1200 and 1400 Ω•m) to cover all extremes. The lower end of the spectrum corresponds to saturated poor-quality concrete, while the higher end of the spectrum corresponds to dry good-quality concrete. Typical values of electrochemical parameters in reference [14, 21-30] are listed in Table 1 and the selected values of electrochemical parameters in this study are listed in Table 2.

3. Parametric study of corrosion rate

Corrosion of steel reinforcement in concrete is a complicated electrochemical process influenced by numerous factors. The thickness of concrete cover, degree of pore saturation (or relative humidity of surrounding environment) and concrete quality (e.g. density or conductivity) not only influence the diffusion and accumulation of gases and ions, lengthen the time of steel depassivation and corrosion initiation, but also impact the limit current density of cathodic reaction and control mode of the corrosion process. Meanwhile, the distribution of corrosion potential within concrete cover is significantly influenced by concrete resistivity and thickness of concrete cover. Furthermore, the anode-to-cathode (A/C)

ratio also has a significant effect on distribution of corrosion potential and corrosion current density. Hence, it is necessary to investigate the influences of A/C ratio, relative humidity, concrete resistivity and thickness of concrete cover on corrosion potential and current density quantificationally before developing the prediction model of corrosion rate.

3.1. Anode-to-cathode ratio

As per conservation of charge, the anodic corrosion current intensity is always equal to cathodic corrosion current intensity for corrosion of steel reinforcement in concrete structures. For a small A/C ratio, the corrosion rate will be higher than that for a large ratio, since the corrosion current density at the anode with a small A/C ratio will be greater than that with a large one for some given current flow associated with the corrosion reaction. Hence, A/C ratio has a significant effect on anodic corrosion current density (or corrosion rate). In fact, A/C ratio is influenced by many factors, such as exposure environment, stress level, crack spread and corrosion product accumulation, *et al*. Generally, corrosion of steel reinforcement induced by carbonation is uniform and its A/C ratio is treated as about 1.0, while corrosion induced by chloride ingress is pitting and the A/C ratio is adopted much smaller than 1.0.

Assuming that cover thickness d=50mm, limit current density i_L=0.4A/m^2, A/C ratio (i.e. $r = L_a / L_c$) varies from 0.1 to 1.0, the influences of A/C ratio on the corrosion potential and current density at the steel surface are shown in Fig. 4. It can be seen from Fig. 4a that both anodic and cathodic corrosion potentials become more and more positive with increase of A/C ratio. As shown in Fig. 4b, the anodic current density increases with the increase of A/C ratio, while the cathodic current density decreases with the increase of A/C ratio. Furthermore, the maximum current density (corresponding to the current density at the transition point between anode and cathode) at the steel surface decreases with the increase of A/C ratio and gradually becomes steady when A/C ratio is relatively large (e.g. r>0.4).

The influences of A/C ratio on corrosion current intensity (I_{corr}) and mean value (i_m) of anodic current density (i.e. corrosion rate) are shown in Fig. 5. It can be seen that I_{corr} increases quickly when A/C ratio is small (e.g. r<0.2) and then gradually stabilizes with an increase in A/C ratio, as shown in Fig. 5a. As shown in Fig. 5b, corrosion rate (i_m) gradually decreases with the increase of A/C ratio. As the A/C ratio increases from 0.1 to 1.0, i_m deceases from about 4.5 to about 1.0, which indicates that the corrosion rate of pitting

corrosion (e.g. $r \leq 0.2$) can be as large as 4.5 times that of uniform corrosion ($r \approx 1.0$).

Distribution of corrosion potential within concrete cover is shown in Fig. 6, taking A/C=0.1 and A/C=1.0 for illustration. If the transition point between anode and cathode is adopted as the reference boundary, the anodic and cathodic potentials become increasingly negative and positive respectively. The distribution of corrosion potential is also a function of the type of corrosion. In the case of uniform corrosion (e.g. r=1.0), the corrosion potential at the concrete surface is generally close to that at the steel/concrete interface; however, in the case of pitting corrosion (e.g. r=0.1), the corrosion potential at the concrete surface can be substantially different from that at the steel/concrete interface. This potential difference is a function of cover thickness and concrete resistivity, and increases with both, which means that typical half-cell potential test technique should be adopted carefully for the pitting corrosion of steel reinforcement in concrete structures [31].

3.2. Relative humidity

Degree of pore saturation in concrete is inherently connected with the relative humidity of surrounding environment and their relationship in the natural environment has been proposed in [32, 33]. Degree of pore saturation impacts the limit current density and finally the corrosion rate via influencing diffusion and concentration distribution of oxygen within concrete cover. Papadakis *et al*. [34] had set up a relationship between effective oxygen diffusion coefficient, concrete porosity and relative humidity as follows

$$D_{O_2} = 1.92 \times 10^{-6} \times \varepsilon^{1.8} \times \left(1 - \frac{r_h}{100}\right)^{2.2} \tag{13}$$

where D_{O_2} is the effective diffusion coefficient of oxygen within concrete (m^2/s); ε is the concrete porosity; r_h is the relative humidity (%).

According to the Eqs. (11) and (13), the influences of relative humidity and cover thickness on the limit current density are shown in Fig. 7. It can be seen that the limit current density decreases with the increase of relative humidity or cover thickness.

The influences of relative humidity on corrosion potential and current density at the steel surface are shown in Fig. 8. As shown in Fig. 8a, anodic and cathodic potentials become increasingly negative and positive respectively given the increase of relative humidity.

However, the influence of relative humidity on both anodic and cathodic corrosion potentials is less significant when the relative humidity is small (e.g. $r_h \leqslant 90\%$). As shown in Fig. 8b, both anodic and cathodic current density increases with the decrease of relative humidity and gradually stabilizes when relative humidity is relatively small. According to Figs. 7 and 8, although potential difference between anode and cathode increases with the increment of relative humidity, corrosion current density decreases with the increase of relative humidity. It is because that the limit current density decreases observably with the increase of relative humidity and corrosion of steel reinforcement is mainly controlled by the cathodic reaction (oxygen diffusion) when the relative humidity is relatively high (e.g. $r_h \geqslant 90\%$). It is clear that relative humidity affects the corrosion rate of steel reinforcement significantly, since it influences the diffusion of oxygen within concrete cover and the limit current density of the cathodic reaction.

3.3. Electrical resistivity of concrete

According to electrochemical principles of corrosion, potential difference, resistance between anode and cathode, and polarization are three major influential factors for corrosion of steel reinforcement in concrete structures. Resistance between anode and cathode is dependent on the electrical resistivity of concrete and distance between anode and cathode, since resistance of steel is much less than that of concrete. Electrical resistance of concrete is influenced by many factors, such as W/C ratio, cement content, mineral mixture, age, environmental condition, *et al*. Taking relative humidity, temperature, curing condition, age, chloride content, test condition into account, the DuraCrete [35] proposed an empirical expression of electrical resistivity of the ordinary Portland cement concrete by fitting experimental data as follows

$$\rho=\rho_0 \cdot \left(\frac{t_h}{t_0}\right)^{n_a} \cdot K_t \cdot K_c \cdot K_T \cdot K_r \cdot K_{Cl} \tag{14}$$

where ρ_0 is the electrical resistivity of the ordinary Portland cement measured by the standard test method with W/C ratio=0.5 and age t_0=28; t_h is the hydration time, t_h = 1 year; n_a is the age factor, for the ordinary Portland cement n_a=0.23; K_t, K_c, K_T, K_c and K_{Cl} are influencing factors of test method, curing method, temperature, relative humidity and chloride content

respectively [35].

According to the experimental data provided by the DuraCrete [35], influencing factor of relative humidity (K_t) can be fitted as follows

$$K_r = \frac{1}{-1.3059\left(\frac{r_h}{100}\right)^2 + 3.6050\left(\frac{r_h}{100}\right) - 1.3270} \quad \left(R^2 = 0.99\right) \quad \text{for } 50\% \leqslant r_h \leqslant 100\% \tag{15}$$

The influence of relative humidity on electrical resistivity of concrete is shown in Fig. 9. It can be seen that electrical resistivity of concrete decreases rapidly with the increase of relative humidity when the relative humidity is smaller than 60% and gradually becomes steady when the relative humidity is larger than about 80%. Meanwhile, electrical resistivity of concrete increases with a decrease in chloride content as chloride ions can enhance conductivity of concrete.

Meanwhile, W/C ratio is another important parameter influencing electrical resistivity of concrete. According to the experimental data reported in literature [36-38], influencing factor of W/C ratio ($K_{\mathrm{W/C}}$) can be fitted as follows

$$K_{\mathrm{W/C}} = \frac{1}{0.0450 + 1.8041\mathrm{W/C}} \quad \left(R^2 = 0.84\right) \tag{16}$$

According to Eq.(16), Eq.(14) can be revised as

$$\rho = \rho_0 \cdot \left(\frac{t_h}{t_0}\right)^{n_a} \cdot K_t \cdot K_c \cdot K_T \cdot K_r \cdot K_{Cl} \cdot K_{\mathrm{W/C}} \tag{17}$$

The influences of chloride content and W/C ratio on electrical resistivity of concrete are shown in Fig. 10. It is clear that electrical resistivity of concrete decreases with the increment of chloride content or W/C ratio, since conductivity and porosity of concrete grow with increase of chloride content and W/C ratio respectively.

The influences of the limit current density and concrete resistivity on corrosion rate (i_m) are shown in Fig. 11. When the limit current density is large (e.g. i_L>0.1A/m^2), the corrosion rate decreases rapidly with the increase of concrete resistivity especially for the small concrete resistivity (e.g. $\rho \leq 400\Omega\bullet\mathrm{m}$), while the limit current density has little influence on the corrosion rate and each of the curves converges towards to an enveloping line, which indicates that corrosion of steel reinforcement is under the resistance control at the moment.

However, when the limit current density is small (e.g. $i_L \leq 0.01 A/m^2$), the corrosion rate doesn't vary with concrete resistivity of range from 50Ω•m to 1400Ω•m, and is equal to that of the limit current density, which means that corrosion of steel reinforcement is under the control of cathodic reaction (oxygen diffusion) right now. For the limit current density given in a specific range (e.g. $0.01 A/m^2 < i_L \leq 0.04 A/m^2$), concrete resistivity doesn't influence the corrosion rate when concrete resistivity is small and corrosion of steel reinforcement is under the control of cathodic reaction (oxygen diffusion). However, with the increase of concrete resistivity the control mode of corrosion is gradually changed from the cathodic control to resistance control. According to above discussions, it is clear that the control mode of corrosion is influenced by both concrete resistivity and the limit current density of the cathodic reaction.

Taking uniform corrosion (e.g. r=1.0) as an example, the influences of concrete resistivity on corrosion potential and current density at the steel surface are shown in Fig. 12. It can be seen that the anodic corrosion potential becomes more and more negative and that of cathode becomes more and more positive with the increase of concrete resistivity, which causes the potential difference between anode and cathode to increase. However, the corrosion current density decreases with an increase of concrete resistivity, since concrete resistance increases much more significantly than that of potential difference.

3.4. Thickness of concrete cover

The influences of concrete cover thickness on corrosion rate (i_m) are shown in Fig. 13. It is clear that corrosion rate increases with the increment of cover thickness when relative humidity is lower than a critical value (e.g. $r_h \leqslant 90\%$), especially for uniform corrosion (e.g. r=1.0). It is because that the supply of oxygen is sufficient to support the cathodic reaction and corrosion of steel reinforcement is under the resistance control when relative humidity is low. At the moment, diffusion passages of both corrosion products and ions increase with the increment of concrete cover thickness, which accelerates corrosion rate of steel reinforcement. On the contrary, corrosion rate decreases with the increase in thickness of concrete cover when relative humidity is fairly high (e.g. $r_h \geqslant 95\%$). It is because that the supply of oxygen in cathode is inadequate for the cathodic reaction and corrosion of steel reinforcement is under the control of cathodic reaction (oxygen diffusion) when relative humidity is relatively high,

and the limit current density decreases with the increment of concrete cover thickness. When relative humidity is within a specific range (e.g. 90%<r_h<95%), corrosion rate increases first and then decreases with the increment of concrete cover thickness, since the control mode of corrosion is gradually changed from resistance control to cathodic control (oxygen diffusion) with the increase of concrete cover thickness.

According to Figs. 11 and 13, it can be concluded that relative humidity doesn't influence the corrosion rate significantly when relative humidity is relatively low (e.g. $r_h \leqslant 90\%$), while the corrosion rate will be influenced markedly when relative humidity is high (e.g. $r_h \geqslant 95\%$). Taking $r_h = 90\%$ and $r_h = 95\%$ as examples, the influences of concrete cover thickness on corrosion potential and current density are shown in Figs. 14 and 15 respectively.

As shown in the Fig. 14, the anodic and cathodic corrosion potential becomes more positive and negative respectively with the increase of concrete cover thickness when relative humidity is 90%. However, corrosion current density increases with an increase of concrete cover thickness, since corrosion of steel reinforcement is under the resistance control when relative humidity is 90% and the concrete resistance decreases with the increment of concrete cover thickness due to more diffusion passages for both corrosion products and ions.

As shown in the Fig. 15, the anodic corrosion potential doesn't vary significantly with concrete cover thickness, but anodic corrosion potential becomes more positive with increase of concrete cover thickness when relative humidity is 95%, which causes the potential difference between anode and cathode to be more larger. However, corrosion current density decreases with the increment of concrete cover thickness, since corrosion of steel reinforcement is under the control of cathodic reaction (oxygen diffusion) when relative humidity is 95% and the limit current density decreases with the increase of concrete cover thickness due to increment of effective thickness of diffusion layer for oxygen.

According to above discussions, control model of corrosion is significantly influenced by both relative humidity and thickness of concrete cover. Corrosion of steel reinforcement is under the resistance control when relative humidity is relative small (e.g. $r_h \leq 90\%$). Regardless of the fact that an increment of concrete cover thickness can prolong the corrosion initiation period, it also reduces concrete resistance due to providing more diffusion passages for corrosion products and ions, which may accelerate the corrosion rate. On the contrary,

corrosion of steel reinforcement is under the control of cathodic reaction when relative humidity is relatively high (e.g. $r_h \geqslant 95\%$), increment of concrete cover thickness will cause increase of effective thickness of diffusion layer for oxygen and decrease of the limit current density, finally slowdown of corrosion rate.

4. Practical model for predicting corrosion rate

4.1. Proposed prediction model

Development of practical prediction model for pitting corrosion rate has its challenges, and research in this area is still being carried out by the authors; therefore the scope of this study is limited to uniform corrosion of steel reinforcement in concrete structures. According to the construction rules of *Chinese Code for Design of Concrete Structures* (GB50010-2010) and *Chinese Code for Durability Design of Concrete Structures* (GB/T50476-2008), it is assumed that thickness of concrete cover varies from 30 to 60mm (4 values: 30, 40, 50 and 60mm), chloride content varies between 0% and 2% (5 values: 0%, 0.5%, 1.0%, 1.5% and 2.0%) and W/C ratio varies from 0.4 to 0.6 (3 values: 0.4, 0.5 and 0.6).

The influences of concrete cover thickness, W/C ratio, chloride content and relative humidity on the corrosion rate are shown in Fig. 16. It is clear that concrete resistivity decreases with the increment of relative humidity, which causes control mode of corrosion gradually changes from resistance control into cathodic reaction control. The relative humidity corresponding to the transition point of control model for corrosion, which is referred as the critical relative humidity, varies from about 85% to 90% [10, 39]. As shown in Fig. 16, corrosion rate (i_m) of steel reinforcement increases with the increments of relative humidity and concrete cover thickness when the relative humidity is lower than the critical relative humidity, since corrosion is under the resistance control at the moment and concrete resistivity decreases with the increase of relative humidity or concrete cover thickness. Meanwhile, corrosion rate increases with increments of W/C ratio and chloride content, because conductivity and porosity of concrete increase with increments of chloride content and W/C ratio respectively. Furthermore, corrosion of steel reinforcement is under the control of cathodic reaction and corrosion rate decreases rapidly with increment of relative humidity when the relative humidity is larger than the critical relative humidity. However, chloride

content and cover thickness have little influence on the corrosion rate at the moment.

Based on above parametric study, engineering parameters such as W/C ratio, chloride content, thickness of concrete cover and relative humidity are important parameters for corrosion control mode and corrosion rate of steel reinforcement in concrete structures. A practical model for predicting corrosion rate as a function of above easily quantifiable engineering parameters is proposed based on a comprehensive nonlinear regression analysis as follows

$$i_m = a_1 r_h + \frac{1}{a_2 r_h^2 + a_3 r_h} + a_4 \tag{18}$$

where a_i (i=1, 2, 3, 4) is the unknown parameter of prediction model, which can be determined by the least-squares fitting method.

It should be noted that the prediction model expressed by the Eq. (18) is only applicable when relative humidity is between 55% and 95%. Corrosion of steel reinforcement is under resistance control when relative humidity is lower than 55%, while the resistance of dry concrete is very large and steel corrodes very slowly. On the contrary, corrosion of steel reinforcement is under control of cathodic reaction when relative humidity is larger than 95%, while the limit current density of wet concrete is very small and steel corrodes very slowly too. That is to say that the corrosion rate of steel reinforcement in concrete is relatively small and generally can be neglected when relative humidity is lower than 55% or larger than 95%.

4.2. Comparison of prediction models

Several prediction models of corrosion rate in reference are selected to compare and verify the accuracy and practicality of the proposed model in this section. Based on the experimental data of accelerated corrosion with relative humidity of 50%~70%, temperature of 20 ± 2℃, and W/C ratio of 0.5, Alonso *et al*. [11] established a prediction model (denoted as the Alonso model hereafter) of corrosion rate as follows

$$i_m = \frac{k_{corr}}{\rho} \tag{19}$$

where, i_m is the corrosion rate (A/m^2); ρ is the concrete resistivity (Ω•m); k_{corr} is the fitting factor, k_{corr}=3.0 V/m.

Based on electrochemical principles and macrocell corrosion model, Ghods *et al*. [23]

established a prediction model (denoted as the Ghods model hereafter) for corrosion rate by taking concrete resistivity, equivalent diffusion coefficient of oxygen, dissolved oxygen content and thickness of concrete cover into account as follows

$$i_m = -3.70\times10^{-3} + \frac{5.06}{\rho} + \left(\frac{0.33}{\rho} - 3.83\times10^{-4}\right)\cdot\ln\left(D_{O_2}\frac{C_{O_2}^s}{d}\right) \tag{20}$$

where ρ is the concrete resistivity (Ω•m); D_{O_2} is the equivalent diffusion coefficient of oxygen (m^2/s); d is the thickness of concrete cover (m); $C_{O_2}^s$ is the oxygen concentration in concrete pore dissolution (kg/m^3).

Considering the influences of temperature, relative humidity, thickness of concrete cover, concrete resistivity, and limit current density on corrosion rate, Pour-Ghaz *et al*. [22] proposed a model (denoted as the Pour-Ghaz model hereafter) to predict both the mean and maximum corrosion rate of steel reinforcement as follows

$$\begin{pmatrix} i_m \\ i_{\max} \end{pmatrix} = \frac{1}{\tau\rho^{\gamma}}\left(\eta T d^{\kappa} i_L^{\lambda} + \mu T \upsilon^{i_L^{\varpi}} + \theta\left(T i_L\right)^{\vartheta} + \chi\rho^{\gamma} + \zeta\right) \tag{21}$$

where, i_m and i_{max} are the mean and maximum corrosion rate respectively (A/m^2); ρ is the concrete resistivity (Ω•m); d is the thickness of concrete cover (m); T is the absolute temperature (K); i_L is the limit current density (A/m^2); τ、γ、η、κ、λ、μ、υ、ϖ、θ、ϑ、χ、ζ are the fitting factors [21].

Combining the equivalent circuit model and the experimental data of accelerated corrosion, Gulikers [40] proposed a prediction model (denoted as the Gulikers model hereafter) of corrosion rate as follows

$$i_m = \frac{98.6960\times10^{-3}\times F_G^{-0.8125}}{\rho} \tag{22}$$

where, i_m is the corrosion rate (A/m^2); ρ is the concrete resistivity (Ω•m); F_G is the geometry factor, taken as 0.0578 V/m.

In order to demonstrate the effectiveness of the proposed model, four values (30, 40, 50 and 60mm) of concrete cover thickness, two values (0% and 2%) of chloride content, three values (0.4, 0.5 and 0.6) of W/C ratio and typical range (55%~95%) of relative humidity are considered. As shown in Fig. 17, the results predicted by the Gulikers and Ghods models deviate far away from those of other models when thickness of concrete cover is small.

Corrosion rate predicted by the Gulikers or Alonso model increases with the increment of relative humidity all the time, which don't agree with the practical situation. All models except the Ghods model tend to coincide with each other with increase of concrete cover thickness, while results predicted by the Ghods model are always smaller than others. Generally, the model proposed in this paper and the Pour-Ghaz model can rationally reflect the expected relationship between corrosion rate and relative humidity.

A further comparison between the proposed model and the Pour-Ghaz model is shown in Fig. 18. It can be seen that the corrosion rate predicted by the proposed model decreases quickly with the increase of relative humidity and is almost not influenced by the thickness of concrete cover when relative humidity is higher than about 90% and corrosion of steel reinforcement is under control of cathodic reaction, which fully agrees with the practical situation. However, with the increase of concrete cover thickness, the fact that the decrease of critical relative humidity and the expansion of cathodic control zone is not being exhibited clearly by the Pour-Ghaz model. Furthermore, corrosion rate predicted by the Pour-Ghaz model decreases slowly in the cathodic control zone, which could induce overestimation of corrosion rate in the case of high relative humidity (e.g. $90\% \leqslant r_h \leqslant 95\%$).

To sum up, both the Gulikers and Alonso models are only suitable for corrosion under control of cathodic reaction but excluding corrosion under resistance control. The proposed model, the Ghods model and the Pour-Ghaz model all capture the characteristic that corrosion rate increases first and then decreases with the increment of relative humidity, and also describe the transition of control model from resistance control to cathodic reaction control. However, corrosion rate predicted by the Ghods model is generally smaller than those of other models and cannot obviously exhibit the transition point of corrosion control mode. Both the proposed and Pour-Ghaz models overcome above drawbacks of the Ghods model. However, the Pour-Ghaz model overestimates corrosion rate and doesn't clearly reflect the fact that the corrosion rate decreases with the increase of relative humidity in the case of high relative humidity (e.g. $90\% \leqslant r_h \leqslant 95\%$). Comparing with the existing models, the proposed model can rationally reflect the expected influences of concrete resistivity and relative humidity on both the corrosion control mode and the corrosion rate of steel reinforcement in concrete structures.

4.3. Verification of proposed model

As discussed in section 4.2, both the Gulikers and Alonso models are only suitable for corrosion under control of cathodic reaction and they are not considered in the following sections. Experimental data of corrosion for steel reinforcement under control of cathodic reaction and resistance in reference are respectively selected to verify the availability of different prediction models in the following two sections.

4.3.1. Corrosion of steel reinforcement under control of cathodic reaction

Concrete specimens with cover thickness of 40mm, two 12mm diameter steel bars at 100mm spacing and dimensions of 150mm×175mm×1500mm were exposed to marine tidal zone in the Cape Town, South Africa as long as 5 years [41]. All the specimens were cast using the ordinary Portland cement mixed with chlorides (2% by mass of binder) to shorten the time of corrosion activation and two values (0.4 and 0.6) of W/C ratio were adopted. Corrosion rate and concrete resistivity were measured by the coulostatic linear polarization resistance technique (LPR) and the Wenner 4-probe techniques, respectively. The detected relative humidity was generally larger than 90% and corrosion of steel reinforcement is under control of cathodic reaction.

Comparisons between experimental data and predicted results of corrosion rate for steel reinforcement under control of cathodic reaction are shown in Fig. 19. It can be seen that the corrosion rate predicted by the Ghods model is much smaller and the one given by the Pour-Ghods model is much larger than the experimental data as W/C=0.4 or W/C=0.6. However, corrosion rate predicted by the proposed model quite agrees with the experimental data as W/C=0.4 or W/C=0.6, which indicates that the proposed model is accurate and practical for corrosion of steel reinforcement under control of cathodic reaction.

4.3.2. Corrosion of steel reinforcement under resistance control

Tang [42] carried out an one-year accelerated corrosion test on the ordinary Portland cement in different organizations including the Force technology, the SP Swedish National Testing and Research Institute, and the CBI Swedish Cement and Concrete Institute. Concrete specimens were cast with W/C =0.5, and four different chloride contents including 0%, 1.5%, 3%, and 6% by weight of cement. Two plain cool-drawn carbon rebar of 10mm diameter and

100mm spacing were put in the middle of the specimens with dimensions of 250mm×250mm×70mm and concrete cover thickness of 30mm. Corrosion rate was measured by different methods including the galvanostatic pulse (GSP) technique, the linear polarization resistance (LPR) technique and the gravimetric method (GM). Furthermore, according to the polarization time, the GSP was divided into two groups including the GSP1 (polarization time being 5s) and the GSP2 (polarization time being 100s). Test results show that steel reinforcements in specimens without chloride were passive as relative humidity was 95%. Uniform corrosion was found for steel reinforcements in specimens with 1.5% and 3% chloride, while pitting corrosion was found in specimens mixed with 6% chloride.

Comparisons between experimental data and predicted results of corrosion rate for steel reinforcement under resistance control are shown in Fig. 20, when chloride content is 1.5%, 3% or 6% and relative humidity is 85%. It is clear that corrosion of steel reinforcement is under resistance control as relative humidity is 85%. There is a wide range of scatter in the experimental dada measured by different techniques. For all the chloride contents, results achieved by the GSP fluctuate significantly and are much larger than those measured by other methods. Results achieved by the LPR are close to each other for different chloride contents but are much smaller than those tested by other methods when the chloride content is low. Results achieved by the GM for all chloride contents agree with each other well. The GM is usually selected as the benchmark for model verification due to its high accuracy. As shown in Fig. 20, corrosion rates predicted by the proposed model as well as the Ghods and Pour-Ghaz models quite agree with the results obtained by the GM for all cases, which means that above three prediction models are accurate and practical for corrosion of steel reinforcement under resistance control.

5. Conclusions

Based on electrochemical principles and macrocell corrosion model, a practical model for predicting corrosion rate of steel reinforcement in concrete structures was proposed with easily quantifiable engineering parameters, such as W/C ratio, chloride content, thickness of concrete cover and relative humidity. According to the model comparison and experimental verification, the following conclusions can be drawn:

(1) Model comparison and experimental verification demonstrate that the proposed prediction model of corrosion rate captures the expected behaviour of corrosion for steel reinforcement in different situations with desirable accuracy and practicality.

(2) Both concrete resistivity and relative humidity have significant influences on the

corrosion control mode and the corrosion rate of steel reinforcement in concrete structures. If relative humidity is relatively low and the limit current density is relatively large, corrosion rate is mainly influenced by concrete resistivity and corrosion is under resistance control; as relative humidity exceeds a critical value, the limit current density is relatively small and corrosion is mainly under control of cathodic reaction even if concrete resistivity varies within a wide range; if relative humidity is within a specific range, the control mode of corrosion is gradually changed from cathodic control (oxygen diffusion) to resistance control with the increase of concrete resistivity. Furthermore, corrosion rate increases with the increment of relative humidity when corrosion is under resistance control, while corrosion rate will decrease with the increment of relative humidity if corrosion is under control of cathodic reaction.

(3) Although an increment of concrete cover thickness can prolong the corrosion initiation period, it also reduces concrete resistance due to providing more diffusion passages for corrosion products and ions, which may accelerate corrosion rate depending on the relative humidity. When relative humidity is lower than a critical value (e.g. $r_h \leqslant 90\%$), corrosion of steel reinforcement is under resistance control and corrosion rate increases with the increment of concrete cover thickness; on the contrary, corrosion of steel reinforcement is under the control of cathodic reaction (oxygen diffusion) and corrosion rate decreases with the increment of concrete cover thickness when relative humidity is relatively high (e.g. $r_h \geqslant 95\%$); furthermore, control mode of corrosion for steel reinforcement gradually changes from resistance control to cathodic reaction control and corrosion rate increases first and then decreases with the increment of concrete cover thickness when relative humidity is within a specific range (e.g. $90\% < r_h < 95\%$).

(4) Distribution of corrosion potential is a function of the type of corrosion (e.g. uniform or pitting corrosion). In the case of uniform corrosion, the corrosion potential at the concrete surface is generally close to that at the steel/concrete interface; however, in the case of pitting corrosion, the corrosion potential at the concrete surface can be substantially different from that at the steel/concrete interface. This potential difference is a function of cover thickness and concrete resistivity, and increases with both, which means that typical half-cell potential test technique should be adopted carefully for pitting corrosion of steel reinforcement in concrete structures.

Acknowledgements

The first author gratefully acknowledges Prof. H. P. Hong at The University of Western Ontario for his collaboration on developing the methodology described above. The financial support received from the National Natural Science Foundation of China (51168003, 51368006), the Technology Foundation for Selected Overseas Chinese Scholar, Ministry of Human Resources and Social Security of China (2012-258), the Major Project of Guangxi Natural Science Foundation (2012GXNSFEA053002), the Guangxi Natural Science Foundation (2013GXNSFBA019237), the Guangxi Science and Technology Development Program (1377001-11) and the Research Program of Science and Technology of Guangxi Higher Education (2013YB009) is gratefully acknowledged.

References

[1] Ghods P, Isgor O B, Pour-Ghaz M. A practical method for calculating the corrosion rate of uniformly depassivated reinforcing bars in concrete. Mater Corros 2007;58(4): 265-272.

[2] Otieno M B, Beushausen H D, Alexander M G. Modelling corrosion propagation in reinforced concrete structures – A critical review. Cement Concrete Comp 2011; 33(1): 240-245.

[3] Shi J J, Sun W. Models for corrosion rate of steel in concrete–A short review. J Chinese Ceram Soc 2012; 40(4): 620-630.

[4] Liu T, Weyers R W. Modeling the dynamic corrosion process in chloride contaminated concrete structures. Cement Concrete Res 1998; 28(3): 365-379.

[5] Scott A N, Alexander M G. The influence of binder type, cracking and cover on corrosion rates of steel in chloride contaminated concrete. Mag Concrete Res 2007;59(7):495-505.

[6] Jiang D W, Li G, Yuan Y S. Experimental studies to the corrosion rate of rebar in concrete. Concrete 2004; 7(1): 3-4+11.

[7] Yu H Y, Zhang H, Wang Q, *et al*. Forecast model of steel corrosion rate of marine concrete. J Build Mater 2009; 12(4): 478-481+492.

[8] Zhu X E, Xie H C. Relationship of reinforcement corrosion parameters and calibration with the losing weight method. Ind Constr 2007; 37(12): 104-108.

[9] Vu K A T, Stewart M G. Structural reliability of concrete bridges including improved

chloride-induced corrosion models. Struct Saf 2000; 22(4):313-333.

[10] Huet B, L'hostis V L, Santarini G, *et al*. Steel corrosion in concrete: Determinist modeling of cathodic reaction as a function of water saturation degree. Corr Sci 2007; 49(4):1918-1932.

[11] Alonso C, Andrade C, Gonzalez J A. Relation between resistivity and corrosion rate of reinforcements in carbonated mortar made with several cement types. Cement Concrete Res 1988; 18(5): 687-698.

[12] Stern M. A method for determine corrosion rates from linear polarization data. Corrosion 1957; 14(9): 440-444.

[13] Raupach M, Gulikers J. A simplified method to estimate corrosion rates - A new approach based on investigations of macrocells. Proceedings of the 8th International Conference on Durability of Buliding Materials and Components, Vancouver, Canada, 1999.

[14] Isgor O B, Razaqpur A G. Modelling steel corrosion in concrete structures. Mater Struct 2006; 39(3): 291-302.

[15] Li F M, Yuan Y S, Ji Y S, *et al*. The corrosion kinetics of steel bars embedded in concrete. J China Univ Min Technol 2008; 37(4): 565-569.

[16] Cao C, Cheung M M S, Chan B Y B. Modelling of interaction between corrosion induced concrete cover crack and steel corrosion rate. Corr Sci 2013; 69: 97-109.

[17] Yu B, Wu M, Yang L F. Influence of concrete cover on corrosion mechanism and corrosion rate of steel bars. Ind Constr 2013; accepted.

[18] Sun Y. Steel corrosion and its control. Harbin: Harbin Institute of Technology Press, 2003.

[19] Li D. Principles of electrochemistry. Beijing: Beijing University of Aeronautics and Astronautics Press, 2008.

[20] Polder R. RILEM TC 154-EMC: Test methods for on site measurement of resistivity of concrete. Mater Struct 2000; 33(234): 603-611.

[21] Ge J, Isgor O B. Effects of Tafel slope, exchange current density and electrode potential on the corrosion of steel in concrete. Mater Corros 2007; 58(8): 573-582.

[22] Pour-Ghaz M, Isgor O B, Ghods P. The effect of temperature on the corrosion of steel in

concrete. Part 1: Simulated polarization resistance tests and model development. Corros Sci 2009; 51(2):415-425.

[23] Ghods P, Isgor O B, Pour-Ghaz M. Experimental verification and application of a practical corrosion model for uniformly depassivated steel in concrete. Mater Struct 2008;41(7):1211–1223.

[24] Kim C Y, Kim J K. Numerical analysis of localized steel corrosion in concrete. Const Build Mater 2008;22(6): 1129-1136.

[25] Kranc S C, Sagues A A. Detailed modeling of corrosion macrocells on steel reinforcing in concrete. Corros Sci 2001;43(7): 1355-1372.

[26] Warkus J, Brem M, Raupach M. BEM-models for the propagation period of chloride induced reinforcement corrosion. Mater Corros 2006;57(8): 636-641.

[27] Redaelli E, Bertolini L, Peelen W, *et al*. FEM-models for the propagation period of chloride induced reinforcement corrosion. Mater Corros;2006:57(8):628-635.

[28] Warkus J, Raupach M. Numerical modelling of macrocells occurring during corrosion of steel in concrete. Mater Corros 2008; 59(2):122-130.

[29] Gulikers J, Raupach M. Numerical models for the propagation period of reinforcement corrosion. Mater Corros 2006;57(8):618-627.

[30] Li F M, Yuan Y S, Geng O, *et al*. Theoretical models of corrosion rate of steel bars embedded in concrete. J S China Univ Technol (Nat Sci Edit) 2009; 37(8): 84-88.

[31] Pour-Ghaz M, Isgor O B, Ghods P. Quantitative interpretation of half-cell potential measurements in concrete structures. J Mater Civil Eng 2009;21(9):467-475.

[32] Ji Y S, Si W, Yuan Y S, *et al*.Experimental research on degree of pore saturation in concrete. Sichuan Build Sci 2010; 36(1): 166-168.

[33] Lu X F, Liu X L, Qin W Z. Moisture distribution of concrete in nature climate. Sichuan Build Sci 2007; 33(5): 114-118.

[34] Papadakis V G, Vayenas C G, Fardis M N. Physical and chemical characteristics affecting the durability of concrete. ACI Mater J 1991;88(2):186-196.

[35] DuraCrete, Statistical Quantification of the variables in the limit state functions. The Netherlands, 2000.

[36] Zhao H B. Research on concrete resistivity and the damage pattern of corroded

reinforced concrete. Ph.D. Thesis, Dalian University Technology, 2008.

[37] Gong G J. Model on the steel corrosion rate in uncracked concrete and patch repair of concrete by chloride ingress. Ph.D. Thesis, Shanghai Jiao Tong University, 2006.

[38] Woelfl G A, Lauer K. The electrical resistivity of concrete with emphasis on the use of electrical resistance for measuring moisture content. Cement Concrete and Aggr 1979;1(2):4.

[39] Enevoldsen J N, Hansson C M , Hope B B. The influence of internal relative humidity on the rate of corrosion of steel embedded in concrete and mortar. Cement and Concrete Res 1994; 24(7): 1373-1382.

[40] Gulikers J. Theoretical considerations on the supposed linear relationship between concrete resistivity and corrosion rate of steel reinforcement. Mater Corros 2005;56(6): 393-403.

[41] Stanish K, Alexander M G. Long term study on chloride and carbonation-induced corrosion of steel in concrete, University of Cape town, 2008.

[42] Tang L P. Calibration of the electrochemical methods for the corrosion rate measurement of steel in concrete. Swedish National Testing and Research Institute, Sweden, 2002.

Figure Captions

Fig. 1. Illustration of macrocell corrosion of steel reinforcement in concrete.

Fig. 2. Macrocell corrosion model of steel reinforcement in RC structure: (a) Illustration of RC beam; (b) Illustration of macrocell corrosion model.

Fig. 3. Flow chart of solution for macrocell corrosion model.

Fig. 4. Influences of A/C ratio on corrosion potential and current density: (a) Corrosion potential; (b) Corrosion current density.

Fig. 5. Influences of A/C ratio on current intensity and mean of current density: (a) Current intensity; (b) Mean of current density.

Fig. 6. Distribution of corrosion potential within concrete cover: (a) r=0.1; (b) r =1.0.

Fig. 7. Influence of relative humidity on the limit current density.

Fig. 8. Influences of relative humidity on corrosion potential and current density: (a) Corrosion potential; (b) Corrosion current density.

Fig. 9. Influence of relative humidity on electrical resistivity of concrete.

Fig. 10. Influences of chloride content and W/C ratio on electrical resistivity of concrete.

Fig. 11. Influences of concrete resistivity and limit current intensity on corrosion rate: (a) r=0.1; (b) r=1.0

Fig. 12. Influences of concrete resistivity on corrosion potential and current density: (a) Corrosion potential; (b) Corrosion current density.

Fig. 13. Influences of concrete cover thickness on corrosion rate: (a) r=0.1; (b) r=1.0.

Fig. 14. Influences of concrete cover thickness on corrosion potential and current density when r_h=90%: (a) Corrosion potential; (b) Corrosion current density.

Fig. 15. Influences of concrete cover thickness on corrosion potential and current density when r_h=95%: (a) Corrosion potential; (b) Corrosion current density.

Fig. 16. Influences of engineering parameters on corrosion rate.

Fig. 17. Comparison of prediction models for corrosion rate: (a) d=30mm ; (b) d=40mm; (c) d=50mm; (d) d=60mm.

Fig. 18. Comparison between proposed and Pour-Ghaz models: (a) Proposed model; (b)

Pour-Ghaz model.

Fig. 19. Verification of prediction models of corrosion rate under control cathodic reaction: (a) W/C=0.4; (b) W/C=0.6.

Fig. 20. Verification of prediction models of corrosion rate under resistance control: (a) C_{cl}=1.5%; (b) C_{cl}=3%; (c) C_{cl}=6%.

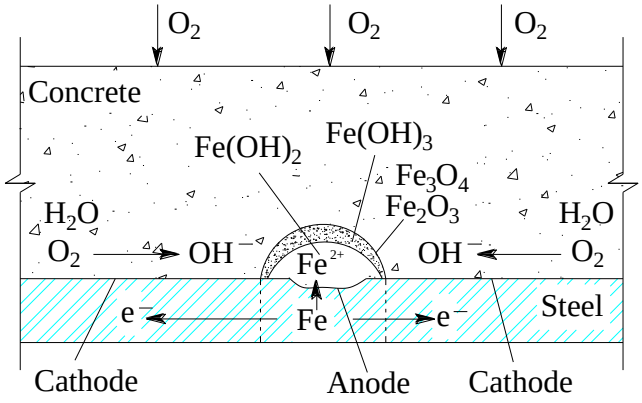

Fig. 1. Illustration of macrocell corrosion of steel reinforcement in concrete.

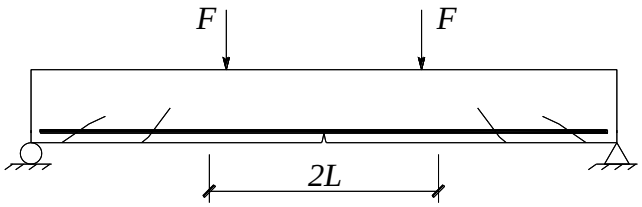

(a) Illustration of RC beam

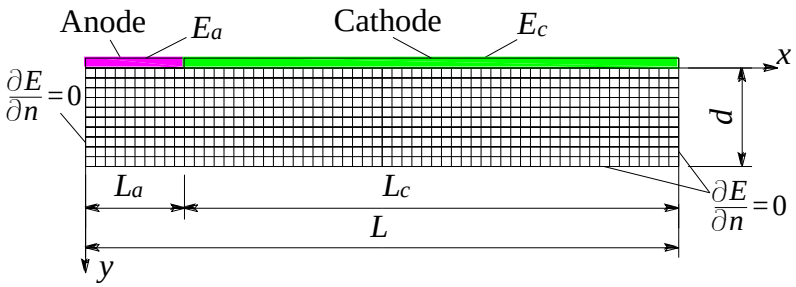

(b) Illustration of macrocell corrosion model

Fig. 2. Macrocell corrosion model of steel reinforcement in RC structure.

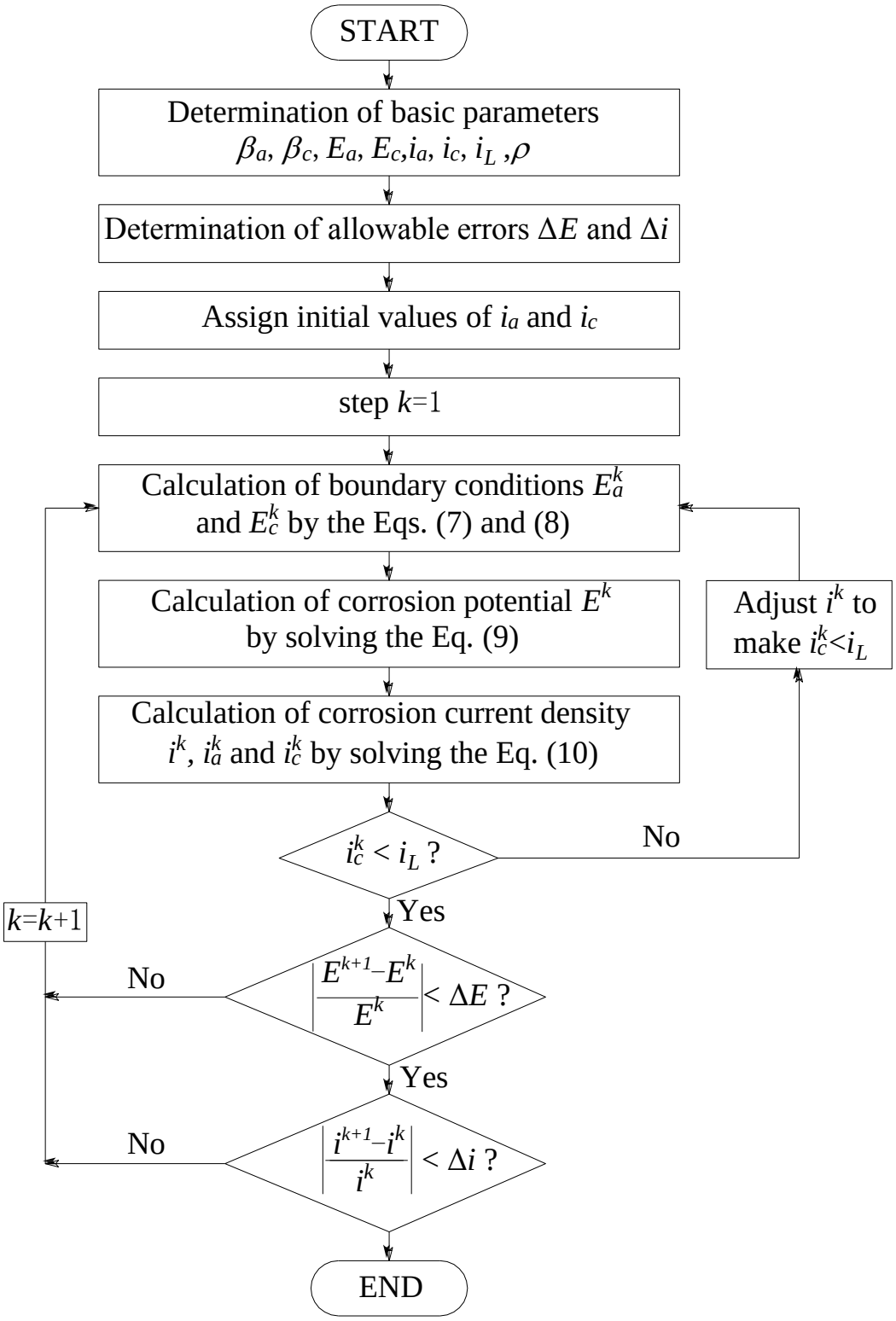

Fig. 3. Flow chart of solution for macrocell corrosion model.

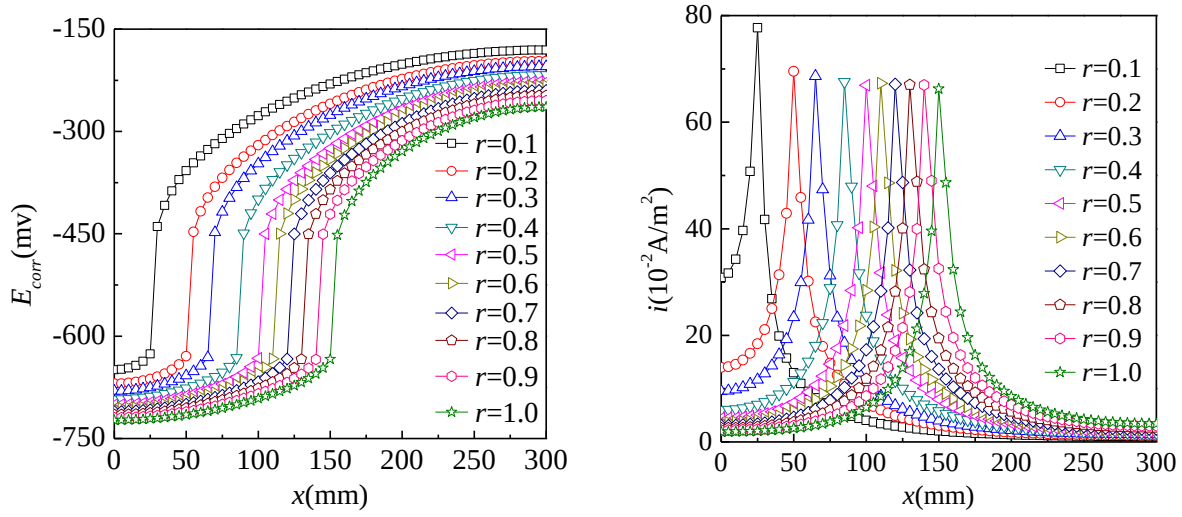

(a) Corrosion potential (b) Corrosion current density

Fig. 4. Influences of A/C ratio on corrosion potential and current density.

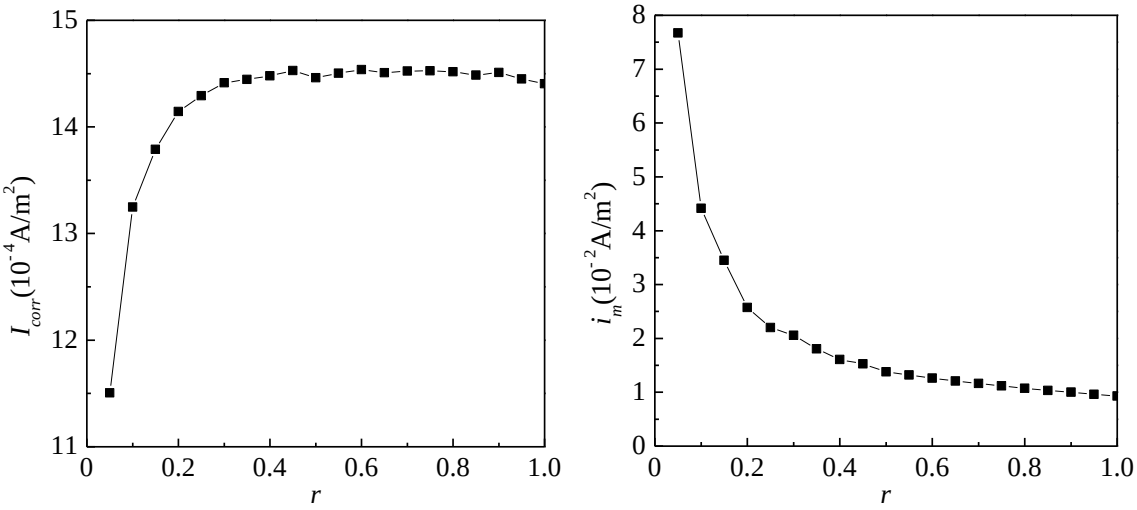

(a) Current intensity (b) Mean of current density

Fig. 5. Influences of A/C ratio on current intensity and mean of current density.

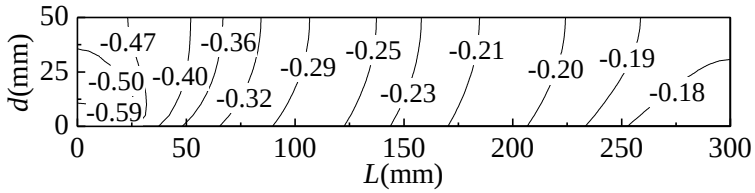

(a) r=0.1

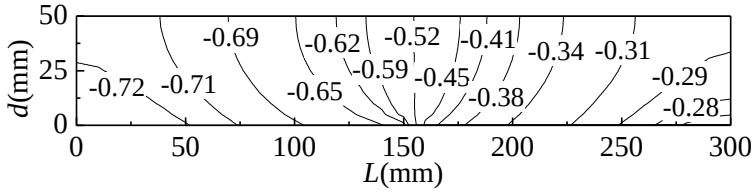

(b) r =1.0

Fig. 6. Distribution of corrosion potential within concrete cover.

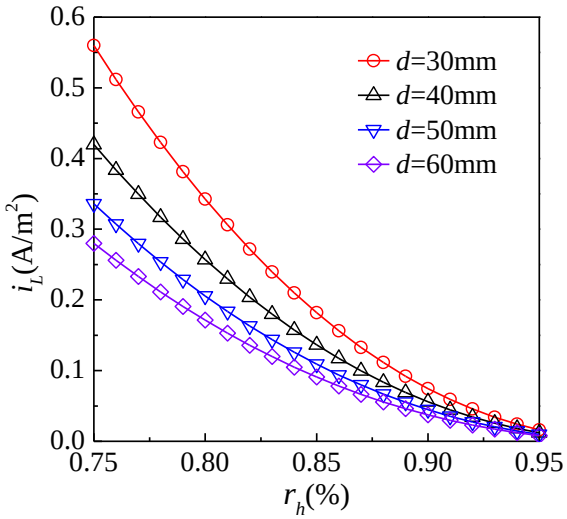

Fig. 7. Influence of relative humidity on the limit current density.

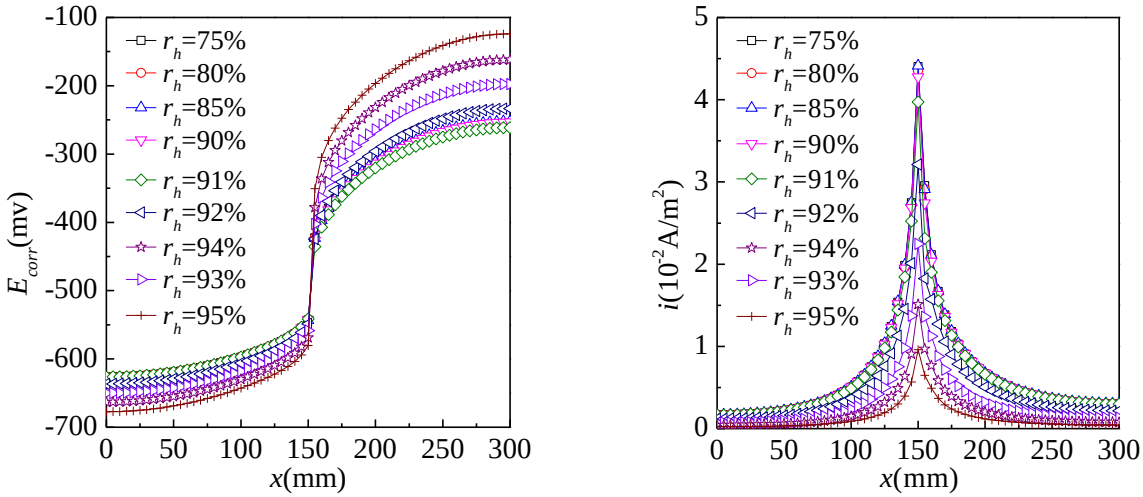

Fig. 8. Influences of relative humidity on corrosion potential and current density.

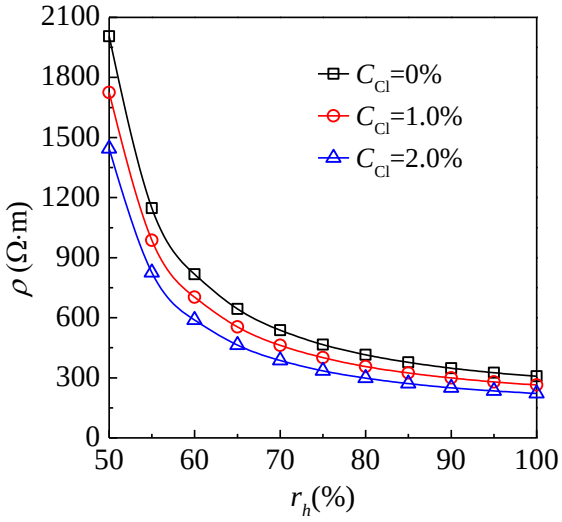

Fig. 9. Influence of relative humidity on electrical resistivity of concrete.

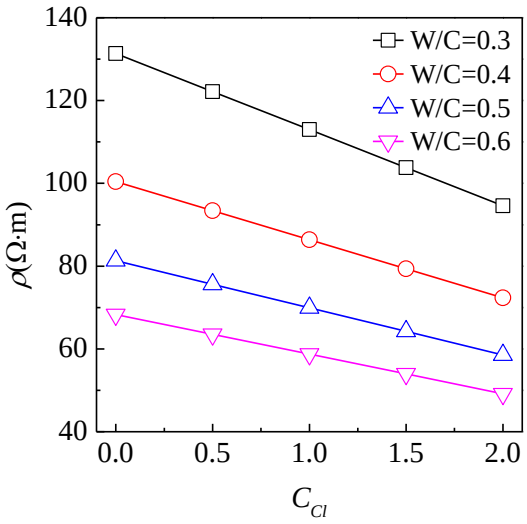

Fig. 10. Influences of chloride content and W/C ratio on electrical resistivity of concrete.

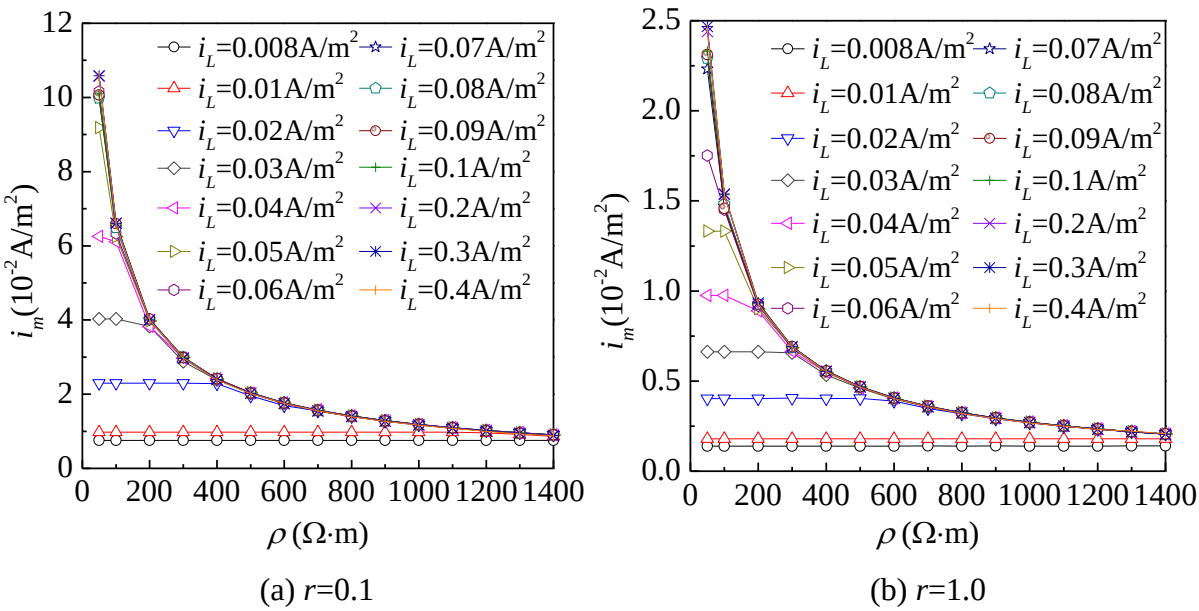

Fig. 11. Influences of concrete resistivity and limit current intensity on corrosion rate.

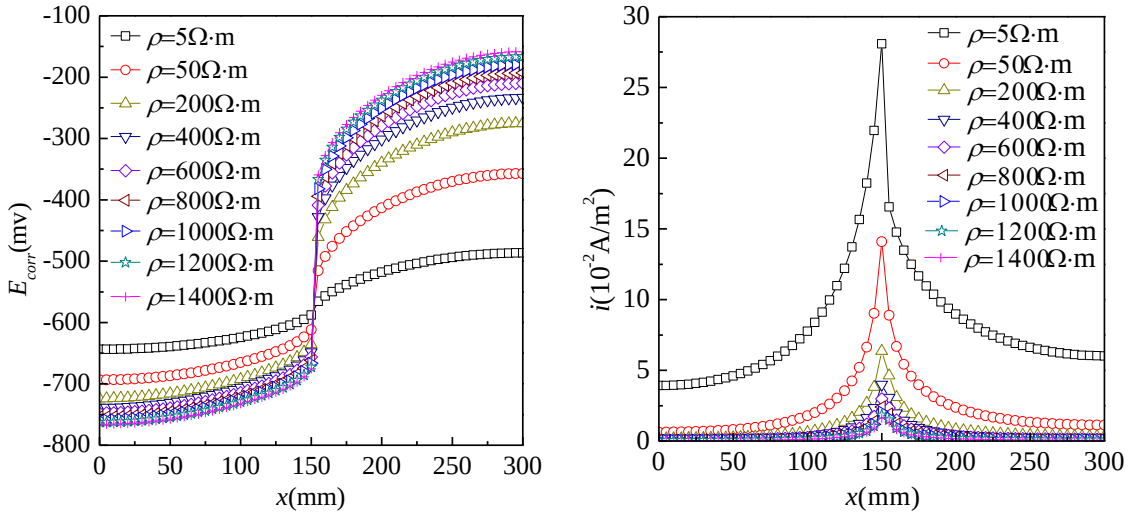

(a) Corrosion potential (b) Corrosion current density

Fig. 12. Influences of concrete resistivity on corrosion potential and current density.

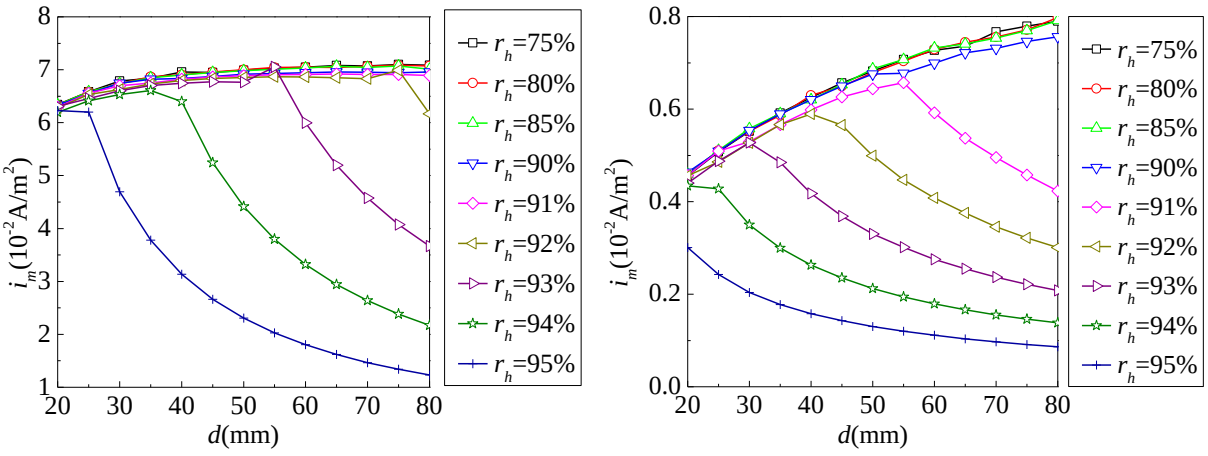

(a) r=0.1 (b) r=1.0

Fig. 13. Influences of concrete cover thickness on corrosion rate.

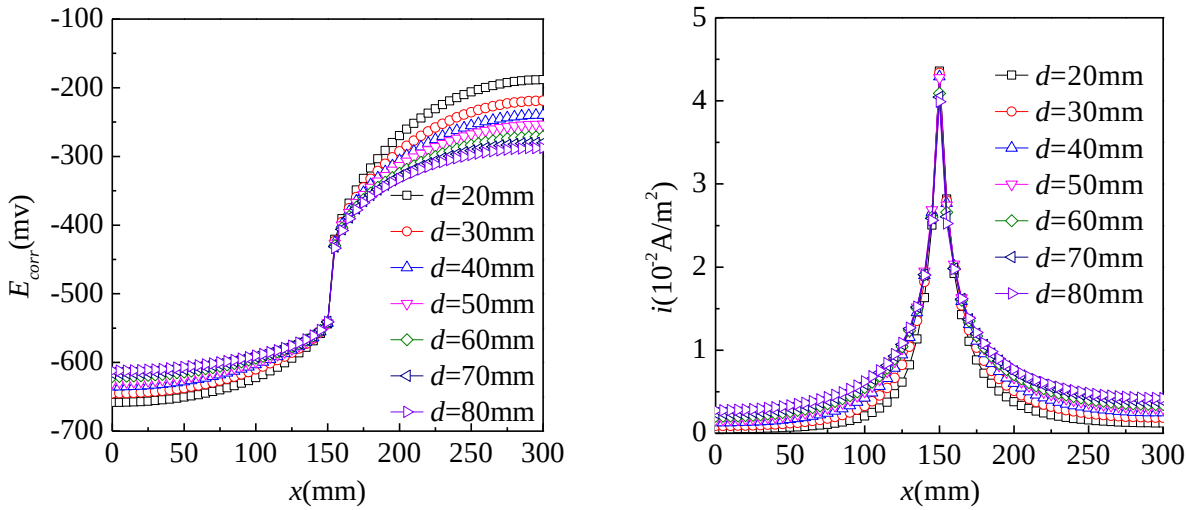

(a) Corrosion potential (b) Corrosion current density

Fig. 14. Influences of concrete cover thickness on corrosion potential and current density when r_h=90%.

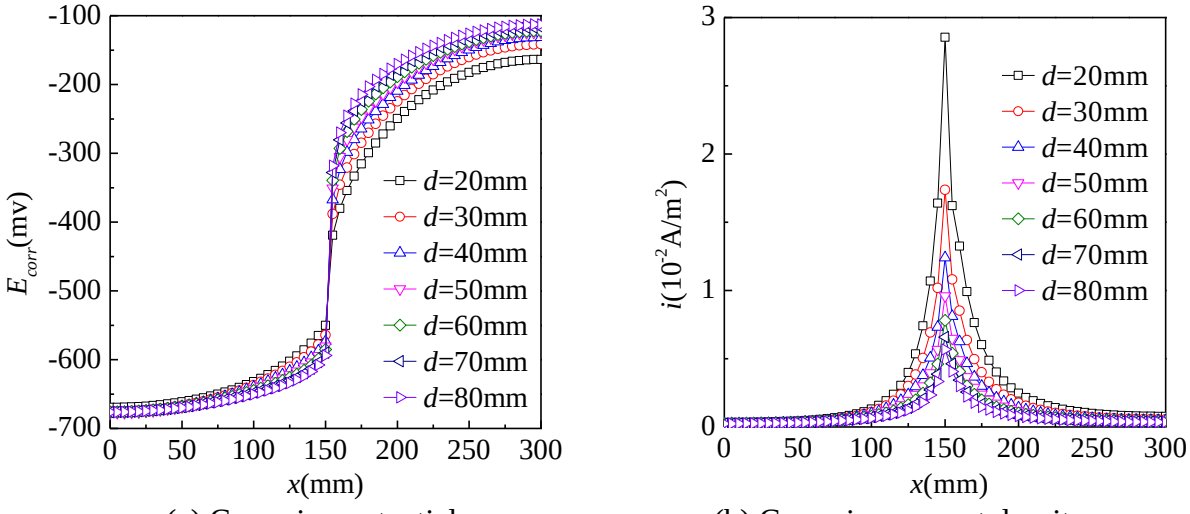

(a) Corrosion potential (b) Corrosion current density

Fig. 15. Influences of concrete cover thickness on corrosion potential and current density when r_h=95%.

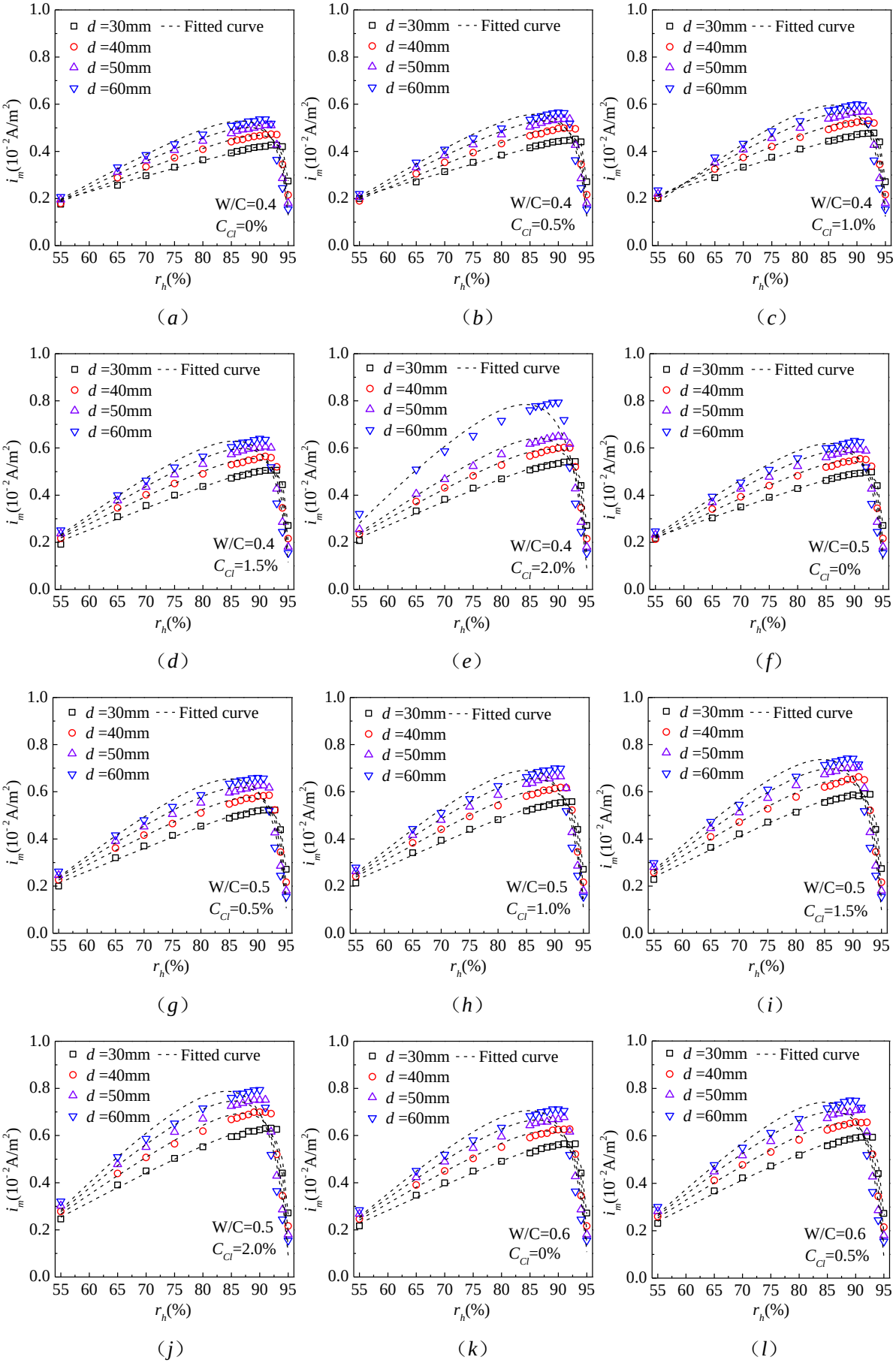
d =30mm
Fitted curve
d =40mm
d =50mm
d =60mm
W/C=0.4
C_Cl=0%
W/C=0.4
C_Cl=0.5%
W/C=0.4
C_Cl=1.0%
W/C=0.4
C_Cl=1.5%
W/C=0.4
C_Cl=2.0%
W/C=0.5
C_Cl=0%
W/C=0.5
C_Cl=0.5%
W/C=0.5
C_Cl=1.0%
W/C=0.5
C_Cl=1.5%
W/C=0.5
C_Cl=2.0%
W/C=0.6
C_Cl=0%
W/C=0.6
C_Cl=0.5%
i_m(10^-2 A/m^2)
r_h(%)
(a)
(b)
(c)
(d)
(e)
(f)
(g)
(h)
(i)
(j)
(k)
(l)

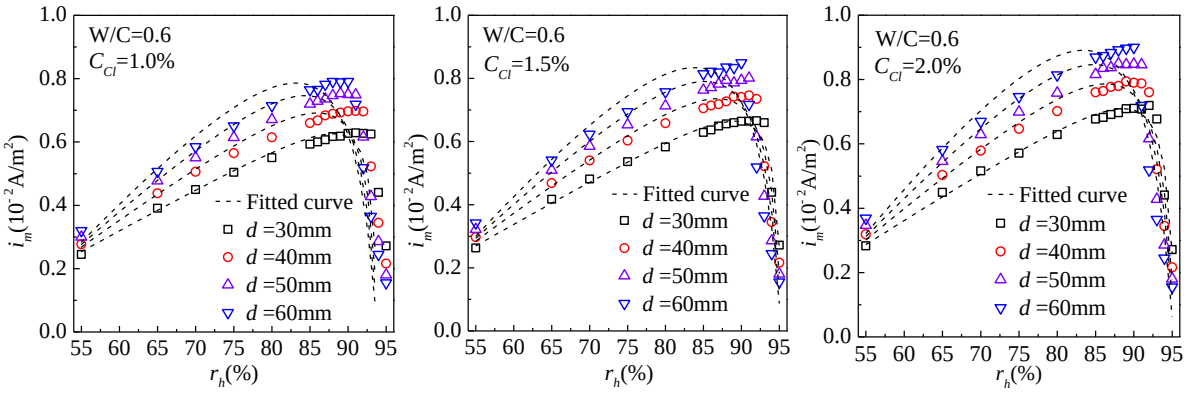

（m）　　（n）　　（o）

Fig. 16. Influences of engineering parameters on corrosion rate.

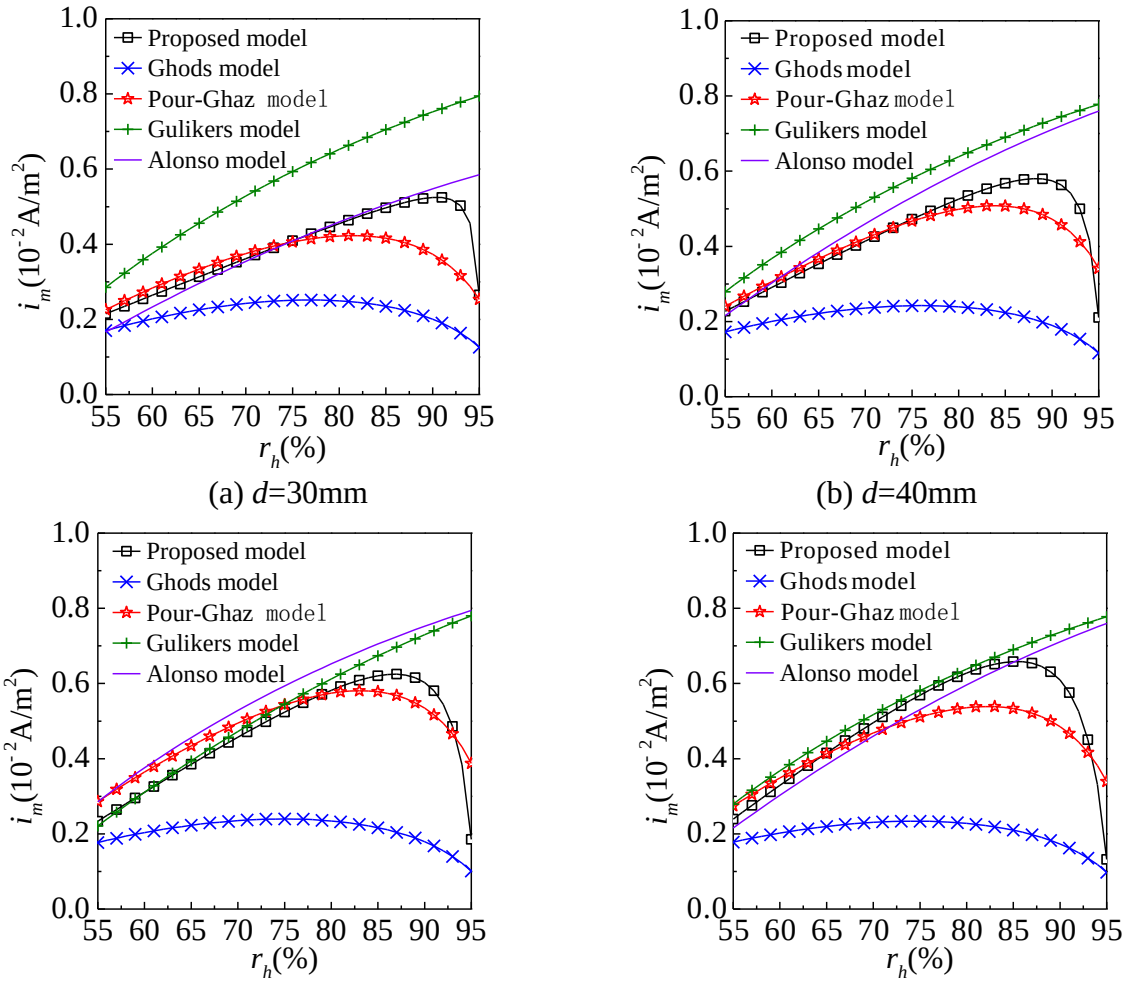

(a) d=30mm (b) d=40mm

(c) d=50mm (d) d=60mm

Fig. 17. Comparison of prediction models for corrosion rate.

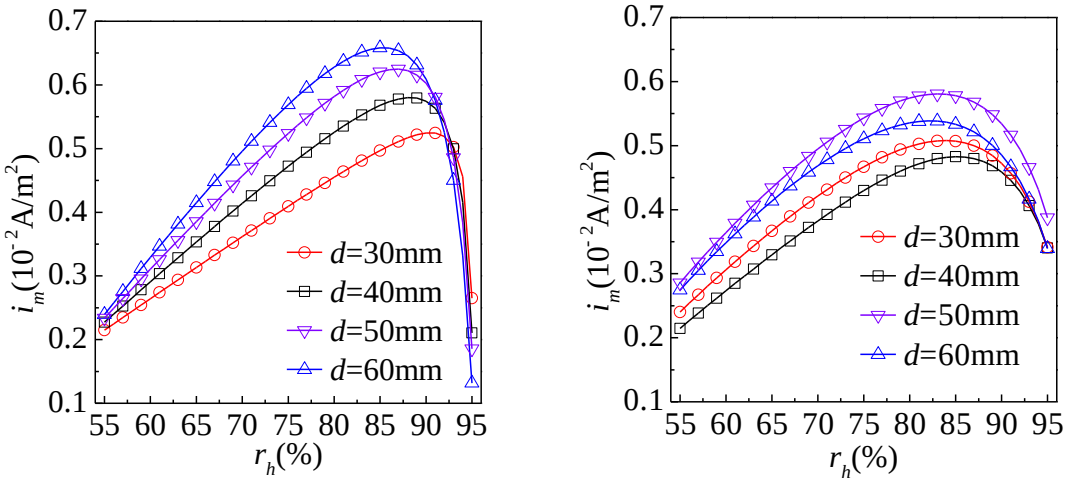

(a) Proposed model (b) Pour-Ghaz model

Fig. 18. Comparison between proposed and Pour-Ghaz models.

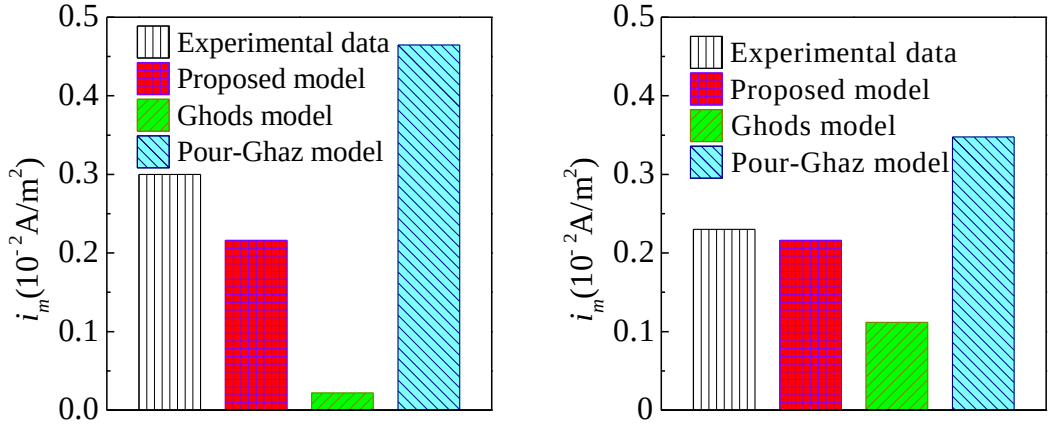

(a) W/C=0.4 (b) W/C=0.6

Fig. 19. Verification of prediction models of corrosion rate under control of cathodic reaction.

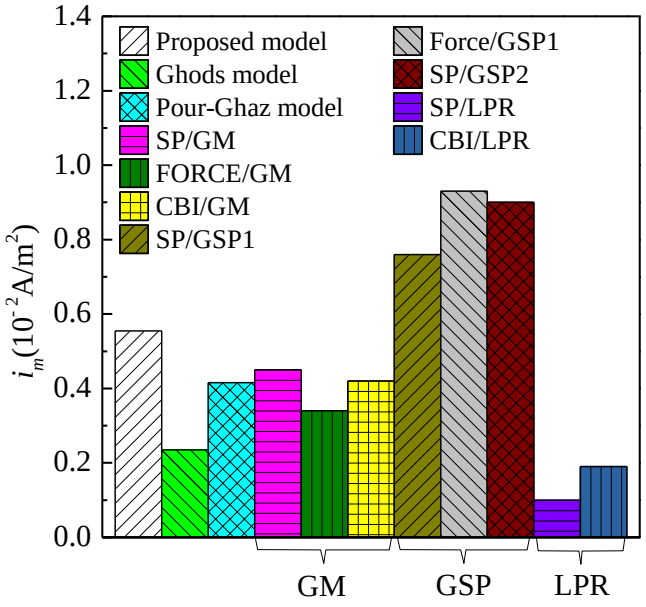

(a) C_{cl}=1.5%

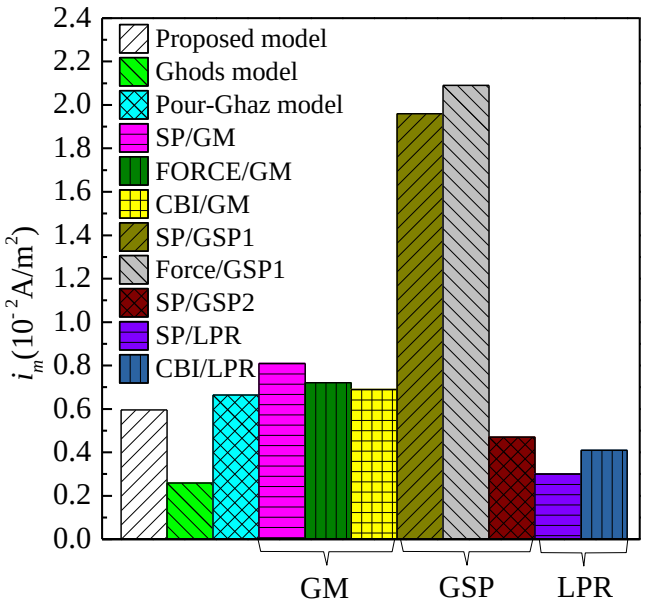

(b) C_{cl}=3%

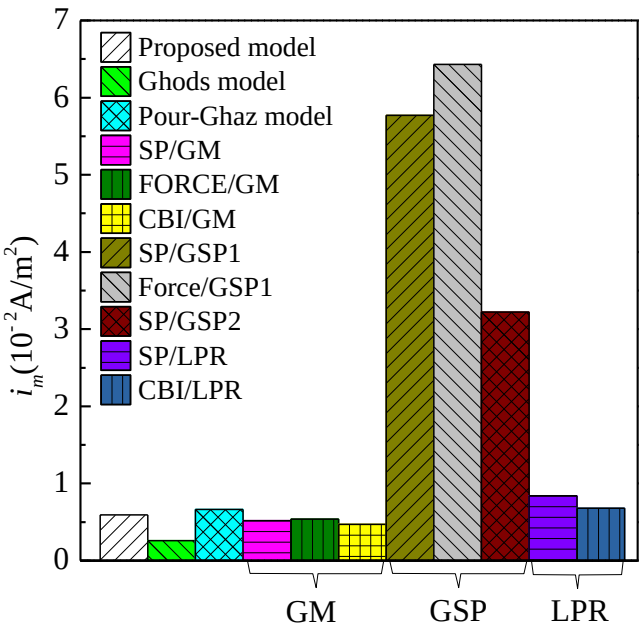

(c) C_{cl}=6%

Fig. 20. Verification of prediction models of corrosion rate under resistance control.

Table Captions

Table 1 Typical values of electrochemical parameters in reference.

Parameter	β_a (mV)	β_c (mV)	i_{oa} (10^{-6}A/m^2)	i_{oc} (10^{-6}A/m^2)	E_{oa} (mV)	E_{oc} (mV)
Isgor and Razaqpur [14]	—	—	275.0	6.0	—	—
Ge and Isgor [21]	60	−160	187.5	6.25	−780	160
Pour-Ghaz and Isgor [22]	90	−180	300.0	10.0	−780	160
Ghods and Isgor [23]	60	−160	300.0	10.0	−780	160
Kim and Kim [24]	90.7	−176.3	275.0	6.0	−690	160
Kranc and Sagues [25]	60	−160	187.5	6.25	−780	160
Warkus *et al.* [26]	100	−200	10000	500	−400	0
Warkus *et al.* [26]	100	−200	10	500	−700	0
Redaelli *et al.* [27]	75	−200	[2500,15000]	100	[−400, −250]	100
Warkus and Raupach [28]	—	−180	—	—	—	—
Brem [29]	75	−200	—	—	−515	−150
Glass [29]	60	−120	100	100.0	−800	100
Gulikers [29]	58.2	−116.3	0.029	0.0028	−1200	400
Peelen [29]	25	−12	10	0.1	−660	−60
Raupach [29]]	0	−176.3	—	—	—	—
Sagues [29]	60	−160	1.48	43.71	−1000	100
Li *et al.* [30]	13	—	1000	—	−680	157

"—" indicates that data is not available in literature.

Table 2 Selected values of electrochemical parameters in this study.

Parameter	Unit	Typical range	Selected value
β_a	mV	60～90.7	60
β_c	mV	−180～−120	−160
i_{oa}	10^{-6}A/m^2	100～300	180
i_{oc}	10^{-6}A/m^2	6～10	6
E_{oa}	mV	−780～−690	−780
E_{oc}	mV	100～160	160

Table 3 Coefficient of prediction model of corrosion rate.

d (mm)	W/C	C_{cl} (%)	a_1 ($\times 10^{-5}$)	a_2	a_3	a_4 ($\times 10^{-3}$)	R^2
		0.0	6.6581	20.5958	-1962.1306	-1.6809	0.9975
		0.5	7.0326	18.2857	-1741.9276	-1.7719	0.9973
	0.4	1.0	7.8317	9.1270	-871.0745	-2.1084	0.9970
		1.5	9.4328	4.7516	-454.6656	-3.0329	0.9932
		2.0	10.3820	3.2720	-313.6121	-3.3740	0.9872
		0.0	8.4513	6.2073	-593.2449	-2.3561	0.9949
		0.5	9.9393	3.7202	-356.3995	-3.2156	0.9905
30	0.5	1.0	10.7761	2.9298	-280.9486	-3.5253	0.9833
		1.5	11.7768	2.1870	-210.0562	-3.8915	0.9774
		2.0	12.8280	1.7764	-170.7514	-4.2683	0.9690
		0.0	11.0642	2.6797	-257.0801	-3.6406	0.9835
		0.5	11.9026	2.1815	-209.4892	-3.9430	0.9764
	0.6	1.0	12.8745	1.7430	-167.5749	-4.2937	0.9704
		1.5	13.9120	1.4319	-137.8018	-4.6515	0.9617
		2.0	15.2480	1.1274	-108.6562	-5.1267	0.9604
		0.0	9.5258	2.6911	-258.4783	-3.2110	0.9740
		0.5	10.2640	2.2371	-215.0490	-3.4902	0.9661
	0.4	1.0	10.8530	1.9104	-183.7677	-3.6111	0.9409
		1.5	12.1940	1.3711	-132.2269	-4.1976	0.9640
		2.0	13.5240	1.0320	-99.7497	-4.6825	0.9626
		0.0	11.8802	1.4829	-142.9189	-4.0820	0.9615
	0.5	0.5	12.9204	1.1773	-113.6657	-4.4755	0.9359
40		1.0	14.0307	0.9453	-91.4265	-4.8743	0.9591
		1.5	15.4172	0.7507	-72.7567	-5.3856	0.9540
		2.0	17.0780	0.5901	-57.3200	-5.9892	0.9489
		0.0	14.3892	0.8821	-85.3703	-4.9987	0.9583
		0.5	15.5575	0.7247	-70.2628	-5.4216	0.9559
	0.6	1.0	16.8791	0.6125	-59.4611	-5.9033	0.9465
		1.5	18.3470	0.5107	-49.6594	-6.4039	0.9377
		2.0	20.3377	0.4022	-39.2170	-7.1106	0.9383
		0.0	11.6560	1.1536	-111.5811	-4.1114	0.9587
		0.5	12.7030	0.9295	-90.0771	-4.5108	0.9539
	0.4	1.0	14.2500	0.7351	-71.4040	-5.2339	0.9323
		1.5	15.0180	0.6369	-61.9290	-5.3206	0.9397
		2.0	16.6940	0.5021	-48.9481	-5.9299	0.9626
		0.0	14.6417	0.6717	-65.2836	-5.1900	0.9428
		0.5	15.7981	0.5701	-55.4881	-5.5987	0.9359
50	0.5	1.0	17.2877	0.4598	-44.8703	-6.1224	0.9399
		1.5	19.0070	0.3648	-35.7153	-6.6895	0.9246
		2.0	20.9973	0.2940	-28.8587	-7.3439	0.9373
		0.0	17.6700	0.4326	-42.2528	-6.2307	0.9402
		0.5	19.1852	0.3565	-34.9094	-6.7392	0.9411
	0.6	1.0	21.0260	0.2942	-28.8864	-7.3779	0.9369
		1.5	22.7162	0.2491	-24.5091	-7.8780	0.9285
		2.0	25.0138	0.2059	-20.3159	-8.6154	0.9221
60	0.4	0.0	13.6260	0.6549	-63.7659	-4.8703	0.9397

	0.5	14.8030	0.5314	-51.8752	-5.2670	0.9415
	1.0	17.9100	0.3706	-36.3868	-6.8634	0.9308
	1.5	17.7100	0.3565	-34.9841	-6.2462	0.9351
	2.0	24.6570	0.1741	-17.2832	-8.3859	0.9626
	0.0	17.3214	0.3738	-36.6597	-6.1261	0.9363
	0.5	18.8520	0.3118	-30.6523	-6.6479	0.9340
0.5	1.0	20.2235	0.2696	-26.5608	-7.0478	0.9237
	1.5	22.3470	0.2170	-21.4547	-7.7178	0.9246
	2.0	24.6569	0.1741	-17.2832	-8.3589	0.9259
	0.0	20.9617	0.2513	-24.7861	-7.3231	0.9234
	0.5	22.5383	0.2142	-21.1769	-7.7774	0.9233
0.6	1.0	24.6501	0.1747	-17.3407	-8.3774	0.9262
	1.5	26.8677	0.1448	-14.4265	-8.9632	0.9223
	2.0	29.5700	0.1182	-11.8192	-9.6336	0.9181